RESEARCH ARTICLE

Tracking the Fragile X Mental Retardation Protein in a Highly Ordered Neuronal RiboNucleoParticles Population: A Link between Stalled Polyribosomes and RNA Granules

Rachid El Fatimy[1,2☯¤a], **Laetitia Davidovic**[3☯], **Sandra Tremblay**[1☯¤b], **Xavier Jaglin**[4], **Alain Dury**[1,2¤c], **Claude Robert**[5], **Paul De Koninck**[1,6], **Edouard W. Khandjian**[1,2]*

1 Institut universitaire en santé mentale de Québec, Quebec, Canada, 2 Département de Psychiatrie et de Neurosciences, Faculté de Médecine, Université Laval, Québec, Quebec, Canada, 3 Institut de Pharmacologie Moléculaire et Cellulaire, UMR7275, Université de Nice-Sophia Antipolis, F-06560 Valbonne, France, 4 Neuroscience Institute, Department of Neuroscience and Physiology, New York University, New York, New York, United States of America, 5 Centre de recherche en biologie de la reproduction, Département des sciences animales, Faculté des sciences de l'agriculture et de l'alimentation, Université Laval, Québec, Quebec, Canada, 6 Département de Biochimie, Microbiologie et Bio-Informatique, Université Laval, Québec, Quebec, Canada

☯ These authors contributed equally to this work.
¤a Current address: Center for Neurologic Diseases, Brigham and Women's Hospital and Harvard Medical School, Harvard Institutes of Medicine, Boston, Massachusetts, United States of America
¤b Current address: Laboratoires de cytogénétique et génétique médicale, Hôpital Saint François d'Assise, le CHU, Québec, PQ, Canada
¤c Current address: Endoceutics Inc, Parc Technologique, Québec, PQ, Canada
* Edward.khandjian@crulrg.ulaval.ca

Abstract

Local translation at the synapse plays key roles in neuron development and activity-dependent synaptic plasticity. mRNAs are translocated from the neuronal soma to the distant synapses as compacted ribonucleoparticles referred to as RNA granules. These contain many RNA-binding proteins, including the Fragile X Mental Retardation Protein (FMRP), the absence of which results in Fragile X Syndrome, the most common inherited form of intellectual disability and the leading genetic cause of autism. Using FMRP as a tracer, we purified a specific population of RNA granules from mouse brain homogenates. Protein composition analyses revealed a strong relationship between polyribosomes and RNA granules. However, the latter have distinct architectural and structural properties, since they are detected as close compact structures as observed by electron microscopy, and converging evidence point to the possibility that these structures emerge from stalled polyribosomes. Time-lapse video microscopy indicated that single granules merge to form cargoes that are transported from the soma to distal locations. Transcriptomic analyses showed that a subset of mRNAs involved in cytoskeleton remodelling and neural development is selectively enriched in RNA granules. One third of the putative mRNA targets described for FMRP appear to be transported in granules and FMRP is more abundant in granules than

in polyribosomes. This observation supports a primary role for FMRP in granules biology. Our findings open new avenues for the study of RNA granule dysfunctions in animal models of nervous system disorders, such as Fragile X syndrome.

Author Summary

Fragile X syndrome is the most common form of inherited mental retardation affecting approximately 1 female out of 7000 and 1 male out of 4000 worldwide. The syndrome is due to the silencing of a single gene, the *Fragile Mental Retardation 1* (*FMR1*), that codes for the Fragile X mental retardation protein (FMRP). This protein is highly expressed in brain and controls local protein synthesis essential for neuronal development and maturation as well as the formation of neural circuits. Several studies suggest a role for FMRP in the regulation of mRNA transport along axons and dendrites to distant synaptic locations in structures called RNA granules. Here we report the isolation of a particular subpopulation of these structures and the analysis of their architecture and composition in terms of RNA and protein. Also, using time-lapse video microscopy, we monitored granule transport and fusion throughout neuronal processes. These findings open new avenues for the study of RNA transport dysfunctions in animal models of nervous system disorders.

Introduction

Neurons are remarkably diverse in shape [1]. They vary from simple unipolar to highly complex multipolar cells, decorated with complex projections of up several centimeters and even one meter in certain cases. Through billions of synaptic connections, these cell-to-cell interactions are the basis for neural circuits that are highly adaptable and functionally autonomous. Their remodelling and adaptation properties contribute to synaptic plasticity [2–5]. These changes rely on rapid local modulation of protein synthesis that is dependent on the presence of the translational machinery and mRNA at the synapse [6]. At the time, the discovery of ribosomal RNA in the axoplasm of the squid giant axon was considered odd and specific to this species [7]. Later, the observation of polyribosome aggregates beneath postsynaptic sites at the base of dendritic spines [8] and in the postsynaptic area of the squid giant synapse [9] convinced scientists that translation could also occur outside of the soma in an autonomous and rapid response to synaptic activity.

Supplying and maintaining subcellular compartments far away from the neuronal soma brings up complex conceptual and biological questions in terms of logistics. Most of protein synthesis takes place in the soma, as the bulk of mRNAs is translated into the cell body. However, a subset of mRNAs is delivered either at presynaptic axonal terminals or at postsynaptic dendritic spines [10,11] where they are further translated into proteins, the synthesis of which is specifically required for adaptation to the local needs of the synapse [12,13]. This extrasomatic targeting of mRNAs allows to rapidly control the synthesis and distribution of the corresponding protein, regulating its level at individual axonal terminals or dendritic spines, in response to external stimuli. The mechanisms of transport, targeting, and release of neurospecific mRNAs at the synapse are gradually being unveiled. While PeriAxoplasmic Ribosomal Plaques (PARPs) corresponding to the translation apparatus have been detected in squid axon [14], RNA granules were observed in the arborisation of neurons in culture [15]. When isolated using sucrose gradients, these granules exhibited sedimentation properties with S values higher

than those of polyribosomes [16]. However, while these granules can be isolated from neurons in primary culture, attempts to purify them from total brain have not been conclusive. Preparations of granules were contaminated by co-sedimentation of other structures such as clathrin-coated vesicles [17] or polyribosomes [18]. Consequently, little is known about the protein and RNA species present in these structures. While mRNAs present in dendrites [11] may possibly be transported in travelling modules, there is no formal biochemical evidence yet for isolated granules. In the present study, we describe a method to isolate and purify RNA granules from mouse brain homogenates, using FMRP as a tracer. Furthermore, we provide a comprehensive proteomic and transcriptomic profiling of mouse brain RNA granules. Finally, we propose a definition of what we consider to be a single granule unit and what we conceive as a cargo of granules.

Results

Isolation of RNA granules from mouse brain

To study the diversity and complexity of neuronal RNA granules, we sought to obtain substantial amounts of these structures. Using mouse brain, we first applied the procedure described by Aschrafi et al. [18] which is based on different sedimentation rates of RNA granules and of polyribosomes [16,19]. Therefore, these two populations can be separated using isokinetic centrifugation through linear sucrose density gradients. Total brain cytoplasmic extracts were prepared without detergent from 10 days-old mice brain, loaded on a 15–30% w/v sucrose gradient over a 70% sucrose pad and centrifuged at 34 000 rpm for 2 hours. Continuous UV monitoring during the course of gradient unloading showed the presence of distinct peaks corresponding to two UV-absorbing populations with different sedimentation properties. A minor peak was observed in the middle of the gradient while a prominent second peak was at the 30–70% sucrose interphase (Fig 1A). According to Ashrafi et al. [18], the latter retains the granules fraction.

To determine the position of polyribosomes in such a shallow sucrose gradient (15–30% w/v), we fractioned the gradient and analysed the distribution of both the ribosomal protein L7 and FMRP, a well-known RNA-binding protein associated to polyribosomes [20,21]. This showed that the minor peak corresponded to monosomes sedimenting at 80S, while most of L7 and FMRP was recovered at the sucrose interface (Fig 1A). These observations strongly suggested that the fraction studied by Ashrafi et al. was unlikely to correspond to granules, as it contained also a high proportion of polyribosomes. Moreover, staining the gel with Coomassie blue showed that the great majority of the sedimenting material was concentrated at the 30–70% sucrose interface (Fig 1A). Finally, electron microscopy of the interface fraction revealed the coexistence of dense amorphous-looking granules and polyribosomes, assembled as beads on a string (Fig 1A). Altogether, this suggested that the method described by Ashrafi et al. was inadequate to separate RNA granules from polyribosomes in mouse brain.

Since discriminating polyribosomes from granules with a 15–30% w/v sucrose density gradient was not possible, we opted for a more standard 15–60% w/v linear gradient over a 70% w/v sucrose cushion. We used brains from P10 mice, since preparing a cytoplasmic fraction enriched in polyribosomes and heavy sedimenting structures is easier at this age [20]. The cytoplasmic sap was ultracentrifuged over a 60% w/v sucrose cushion. The resulting opalescent pellet was resuspended and further analysed by isokinetic centrifugation. Under these conditions, the ribosomal L7 protein and FMRP were detected at the level of polyribosomes (Fig 1B), as previously documented [20,21], indicating that polyribosomes could be separated from the 60–70% sucrose interface. Also, both proteins were present at the 60–70% w/v interface, but penetrated the sucrose cushion as they also appeared in lower fractions. To confirm that the
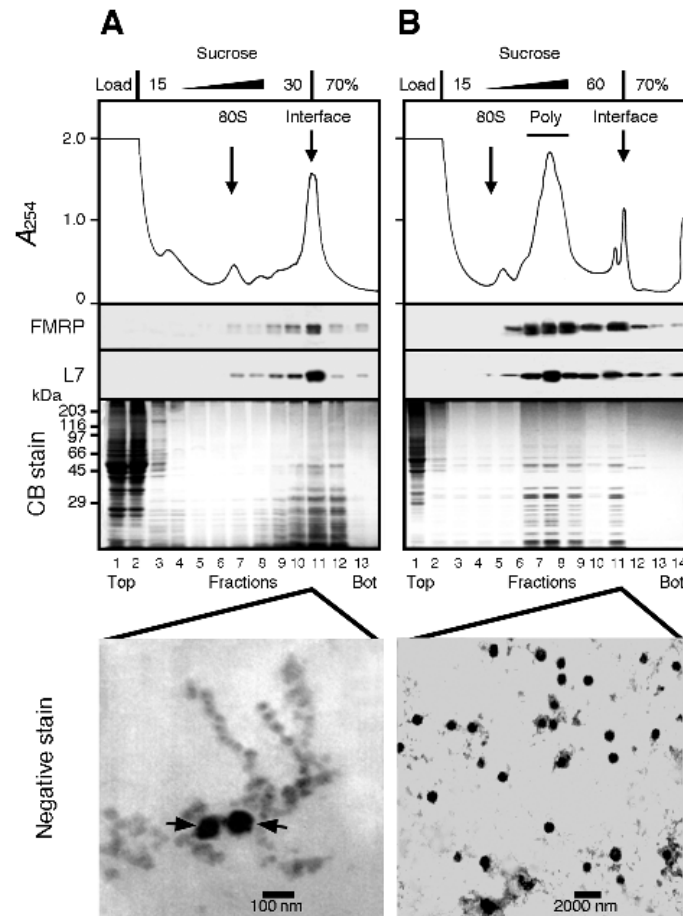
Fig 1. Attempts to separate polyribosomes from heavy sedimenting granules. A) Brain cytoplasmic extract prepared without detergent was analysed by sedimentation velocity throughout a 5–30% (w/v) sucrose density gradient layered over a 70% (w/v) sucrose cushion. The collected fractions were analysed by SDS-PAGE followed by Coomassie blue staining and immunoblotting to detect the ribosomal protein L7 and FMRP. A major UV-absorbing peak is observed at the 30–70% sucrose interface that contained L7 and FMRP. Electron micrographs of this fraction revealed that both beads on a string like structures of polyribosomes and dense amorphous granule-like structures (arrows) were recovered at the interface. **B)** Total polyribosomes from brain cytoplasmic extract were first concentrated by ultracentrifugation, resuspended, and then analysed by sedimentation velocity throughout a 15–60% (w/v) sucrose density gradient layered over a 70% (w/v) sucrose pad. All collected fractions were analysed by Coomassie blue staining after SDS-PAGE, and by immunoblotting to detect the ribosomal protein L7 and FMRP. While polyribosomes were detected in the middle of the gradient, electron micrographs revealed that the sucrose interface fraction contained 100–800 nm diameter granule-like structures. Note the extended scale in **B** as compared to that in panel **A**.

doi:10.1371/journal.pgen.1006192.g001

material present at the interface did correspond to granules, samples were examined by electron microscopy following negative staining. Electron dense round shaped particles ranging from 100 to 800 nm were observed (note the extended scale in Fig 1B as compared to Fig 1A). Altogether, these data demonstrate that a fraction enriched in granules is obtained at the interface under the conditions described here. However, contamination by large sedimenting polyribosomes could not be ruled out because of the close vicinity of the collected fractions. We therefore modified three parameters: 1) we eliminated the sucrose cushion to allow rapidly sedimenting material to concentrate at the bottom of the centrifuge tube; 2) we reduced the centrifugation time down to 45 minutes to separate the polyribosome fractions from heavy
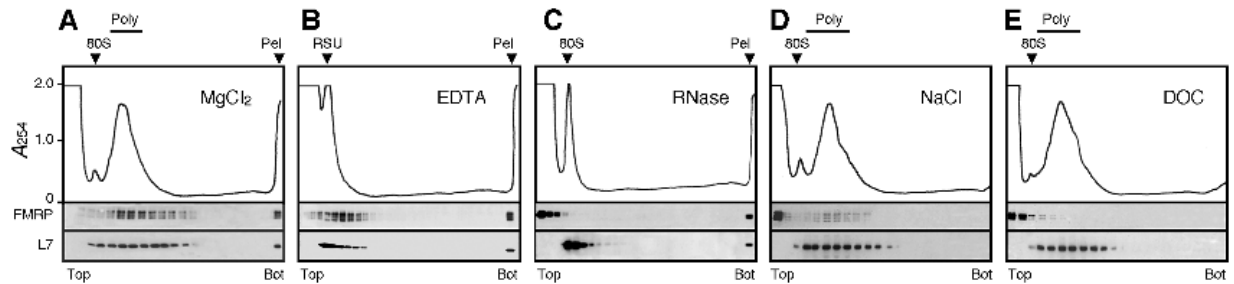
Fig 2. Heavy sedimenting structures are not *bone fide* polyribosomes. Aliquots of concentrated polyribosomes were analysed by sedimentation velocity through 15–60% (w/v) sucrose density gradients. **A)** In the presence of MgCl₂, FMRP was detected at the level of polyribosomes (Poly) and the pellet fraction (Pel). After incubation with 30 mM EDTA (**B**) or treatment with 10 µg/ml RNase A (**C**), a clear displacement of the ribosomal L7 protein and FMRP towards the top of the gradient was observed, while both proteins were still detectable in the pellet (Pel). Conversely, in the presence of 0.4 M NaCl (**D**) or the anionic detergent deoxycholate (DOC, **E**), the majority of FMRP was found in the loading volume that did not penetrate the gradient, while the polyribosomal UV profile remained unchanged. In these conditions no UV-absorbing materials as well as no FMRP or L7 were detected in the pellet fraction.

doi:10.1371/journal.pgen.1006192.g002

sedimenting structures, and 3) we unloaded the sucrose gradient from the top using the Auto Densi-Flow (Buchler) rather than piercing the tube, thus protecting the integrity of the pellet. These adjustments, allowed the separation of polyribosomes from heavy sedimenting structures containing L7 and FMRP, which were recovered at the bottom of the tube (Fig 2A).

The presence of structures sedimenting faster than polyribosomes, suggested that this pellet fraction corresponded either to granules or polyribosomes aggregates. To discriminate between these two structures, polyribosome-enriched extracts were submitted to different treatments prior to velocity sedimentation through sucrose density gradients. An EDTA treatment, which dissociates polyribosomes into their ribosomal subunits (RSU), and an RNAse treatment, that completely destroys polyribosomes had no effect on the presence of FMRP and L7 in the pellet (Fig 2B and 2C). This suggested that these heavy-sedimenting structures did not correspond to classical *bone fide* polyribosomes. We then tested the effect of high-salt conditions (0.4 M NaCl) on the material contained in the pellet. We observed that approximately 50 to 70% of FMRP was removed from polyribosomes and was recovered at the top of the gradient, while the rest of FMRP remained associated with polyribosomes (Fig 2D), as previously reported [22]. Under these high-salt conditions, we neither detected a visible pellet, nor recovered UV absorbing material or FMRP and L7 at the bottom of the tubes (Fig 2D). Similarly, while treatment with the anionic detergent deoxycholate (DOC) did not affect the polyribosomal UV profile, it eliminated UV absorbing material from the pellet (Fig 2E). This is in agreement with previous studies showing that FMRP together with other proteins, is stripped off polyribosomes by DOC [20,21,23]. These observations strongly suggested that the material recovered at the bottom of the tubes present a tertiary structure different from classical polyribosomes.

We then performed electron-microscopy analyses to visualize the components present in the pellet and in the polyribosomal fractions (Fig 3A). Electron micrographs of polyribosomal fractions revealed the typical appearance of polyribosomes with ribosomes assembled on mRNA as beads on a string, while clumps of amorphous structures were visible in the resuspended pellet fractions. We hypothesized that these aggregates were due to the high g forces generated during ultracentrifugation, compacting the particles against the tube bottom wall. We therefore added a step in which the pellet was dispersed by two short bursts of ultra-sonication. Following that treatment, the structures present in the pellet fraction appeared as a heterogeneous set of small granules with size ranging from 100 to 300 nm (Fig 3B). Higher magnification revealed a morula-like structure of granules, each formed of round units of 25 nm in diameter similar to ribosomes [24] (Fig 3C). Quantification in an array of 350 granules

showed that the number of units present in a single granule range from 5 to 20 (Fig 3C and 3D). Because EM preparations tend to flatten structures, we hypothesized that the number of ribosomal units was underestimated. Indeed, 3D reconstruction models revealed the hidden face of the preparations. Thus, granules estimated to contain 7 ribosomes, might in fact accommodate 12 to 13 units (Fig 3E). Immunogold labelling on ultra-thin sections of LR-White resin embedded granules with antibodies against the large L7 and the small S6 ribosomal subunit proteins, confirmed that the units composing the granules corresponded to ribosomes (Fig 3F and 3F'). While we expected that all ribosomes contained in a granule would react to the antibodies, these granules were not uniformly labelled. This was probably due to the fact that the protein epitopes were localized above or below the levels of the ultrathin sections. Immunogold labelling of FMRP showed that the protein was not present in all granules (Fig 3G), as it was the case for its two homologues, FXR1P and FXR2P (S1 Fig). The average number of FMRP-gold signals detected in each granule was 3 as determined in n = 100 FMRP positive granules (S2 Fig). However, this number might be underestimated, because the FMRP epitopes might be missing, as is the case for L7 (see above). On the other hand, only 30% of the granules carried FMRP-gold signals. A more detailed quantitative study of the distribution of FMRP in granules, using immunofluorescence approach, is presented below. We observed the presence of granules in the pellets recovered after RNase and EDTA treatments of the cytoplasmic sap (see Fig 2B and 2C). However, we systematically noted that their morphology was slightly altered as less defined images were obtained (Fig 3H and 3H'). Finally, to serve as negative controls, sections were incubated in the presence of the sole secondary gold-labelled antibodies. Occasionally, single gold-particle was observed outside of the granules in different regions of the sections (Fig 3I).

These results collectively suggest that although granules are highly diverse in terms of size and composition, their basic unit remains the ribosome.

Purification of the granules

While the procedures described above were appropriate to obtain fractions highly enriched with granules, we wondered whether they were purified sufficiently for further biochemical studies. Granule fractions obtained as pellets (see Fig 3A) were analysed by SDS-PAGE and their protein composition compared to that of purified polyribosomes. Coomassie blue staining revealed that granules contained a majority of ribosomal proteins. However additional bands were observed, in particular at around 230–100 and 55–40 kDa (Fig 4A, highlighted with stars and in grey area) accounting for 36% of the total protein content as determined after scanning of the stained gels. We hypothesized that these bands would correspond to components of the cytoskeleton framework that might have contaminated the granule preparations. Therefore, we tested for the presence of three main cytoskeletal proteins: the neurofilaments (NF), β-actin and β-tubulin. Immunoblot analyses using antibodies to these proteins confirmed their presence (Fig 4A). This evidenced that cytoskeleton components had contaminated the granule fraction during differential centrifugations. An additional purification step was thus necessary.

Granules and polyribosomes recovered after isokinetic ultracentrifugation in sucrose density gradients (S3A Fig) were subjected to equilibrium (isopycnic) ultracentrifugation in a 10 to 60% w/v Metrizamide linear gradient [25] (S3B Fig). Both structures were detected in fractions with a calculated density of 1.295 g/cm^3, corresponding to the buoyant density of polyribosomes [26]. Centrifugation prolonged for 48 hours did not change the particle density indicating that they have reached their equilibrium density already by 18 hours. FMRP and L7 were systematically detected in fractions corresponding to this density. Coomassie blue staining
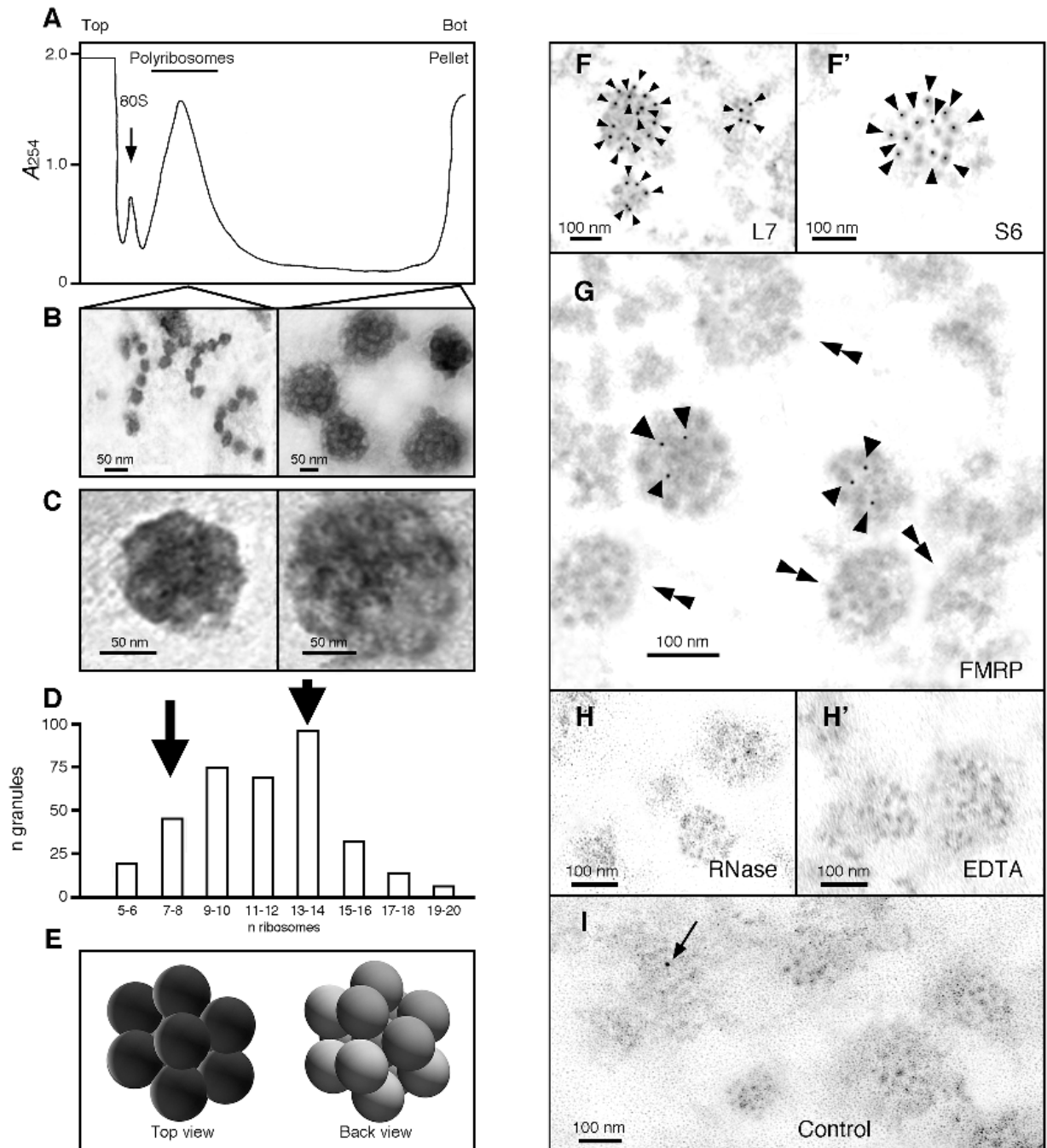
Fig 3. Ribosomes are the basic units of the granules. A) Concentrated samples of polyribosomes were analysed by centrifugation through linear 15–60% (w/v) sucrose gradient, and fractions were collected with continuous monitoring at 254 nm. Reducing the time of centrifugation to 45 min, allowed polyribosomes to be separated from granules that sediment at the bottom of the gradient. **B)** Isolated polyribosomes and granules were observed by electron microscopy after negative staining. While polyribosomes present an open structure similar to beads on a string, granules display a densely compacted morula-like structure. **C)** Shown are two granules of two different sizes. The diameter of each unit composing the granules is similar to the reported size of 25 nm for ribosomes. **D)** Size distribution of granules according to their number of visible units as revealed by negative staining. Quantification of ribosomes present in each granule shows that their number varies from 5 to 20, with a mean average of 9 to14 ribosomes. **E)** 3D model of granules from top and back views suggests that the number of ribosomes observed in flatten EM preparations is under estimated. **F** and **F')** Immunogold labelling of ribosomal protein L7 and S6 (15 nm, arrow heads), and **G)** FMRP (5 nm, arrow heads) in granules; double arrow heads point to granules free of FMRP gold signals. **H** and **H')** RNAse and EDTA treated granules show slightly altered structures. **I)** Control analysis without primary antibodies showing a single contaminant signal (arrow). Ultrathin sections were obtained on materials embedded in LR-White resin.

doi:10.1371/journal.pgen.1006192.g003

Fig 4. Protein analyses of the enriched and purified granules fractions. Distribution of proteins in polyribosomes (P) and granules (G) fractions: **A)** Following centrifugation in sucrose gradient and, **B)** After isopycnic centrifugation in Metrizamide gradients. Coomassie blue staining of proteins separated by SDS-PAGE and their corresponding scans. Immunoblot analyses (I.B.) for both preparations were performed in parallel in the same conditions with identical exposure time to the X ray films.
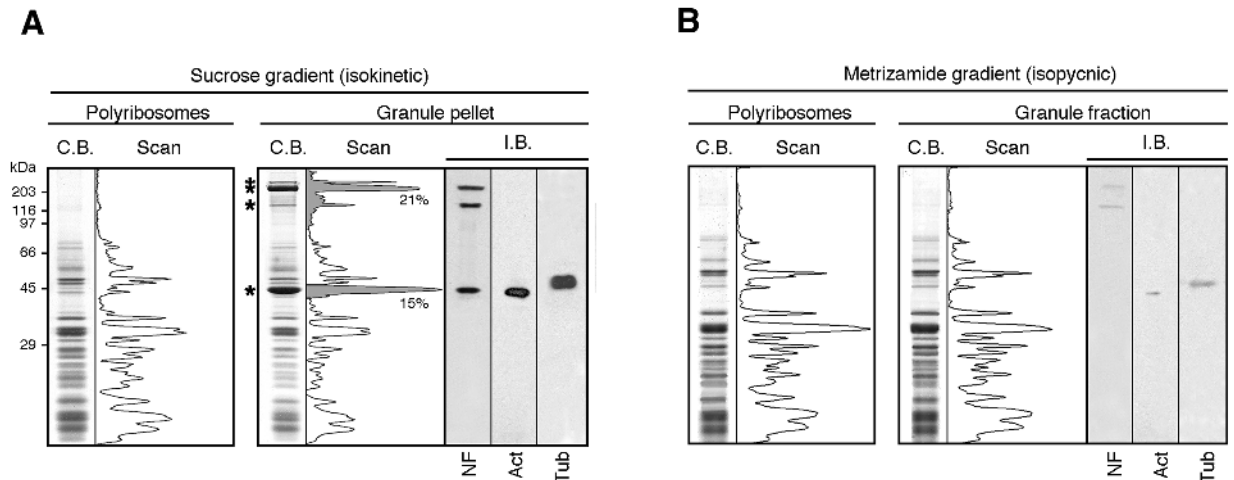
doi:10.1371/journal.pgen.1006192.g004

highlighted that polyribosomes and granules shared common protein profile ([Fig 4B](#)), suggesting similar protein content. More importantly, the contaminant peaks highlighted in gray in [Fig 4A](#) were no longer detected after this additional purification step. To assess the level of purification, we also performed immunoblot analyses and observed a 8-fold decrease in the signals corresponding to neurofilament, actin and tubulin, indicating that the majority of cytoskeletal contaminants were removed by the Metrizamide step.

Altogether, these data showed that the procedure described here enables the isolation of granules from mouse brain with a minimum of contaminants.

Proteomic analyses of granules preparations

To reveal the protein content of polyribosomes and granules purified by isopycnic centrifugation in Metrizamide gradients, fractions were analysed by Mass Spectrometry (MS). A total of 128 proteins sharing at least 1 peptide with known proteins registered in databases were found in granules ([Fig 5](#) and [S1 Table](#)), while 155 proteins were present in polyribosomes. Gene ontology-based pathway enrichment analyses revealed that the most significantly enriched biological processes in granules were notably 'translational elongation' (adjusted p-val = $2,67.10^{-128}$), 'RNA processing' (adjusted p-val = $1,38.10^{-12}$), 'ribonucleoprotein complex biogenesis' (adjusted p-val = $1,41.10^{-12}$) and 'cytoskeleton-dependent intracellular transport' (adjusted p-val = $3,40.10^{-3}$) ([S2 Table](#)). In addition, the most significantly enriched molecular functions in granules were 'structural constituent of ribosome' (adjusted p-val = $2,36.10^{-98}$), 'RNA binding' (adjusted p-val = $2,65.10^{-64}$), 'translation regulator activity' (adjusted p-val = $4,11.10^{-2}$) or 'structural constituent of cytoskeleton' (adjusted p-val = $1,42.10^{-2}$). The same analyses performed on the 155 proteins identified in polyribosomes highlights essentially the same classes of biological processes linked to 'translation', 'ribosome' or 'RNA binding' ([S3 Table](#)). However, cytoskeleton-related processes were not significantly enriched in the polyribosomal protein pool, suggesting that the main divergences observed with polyribosome and granule preparations expressed in terms of protein content, belong to this class of processes.
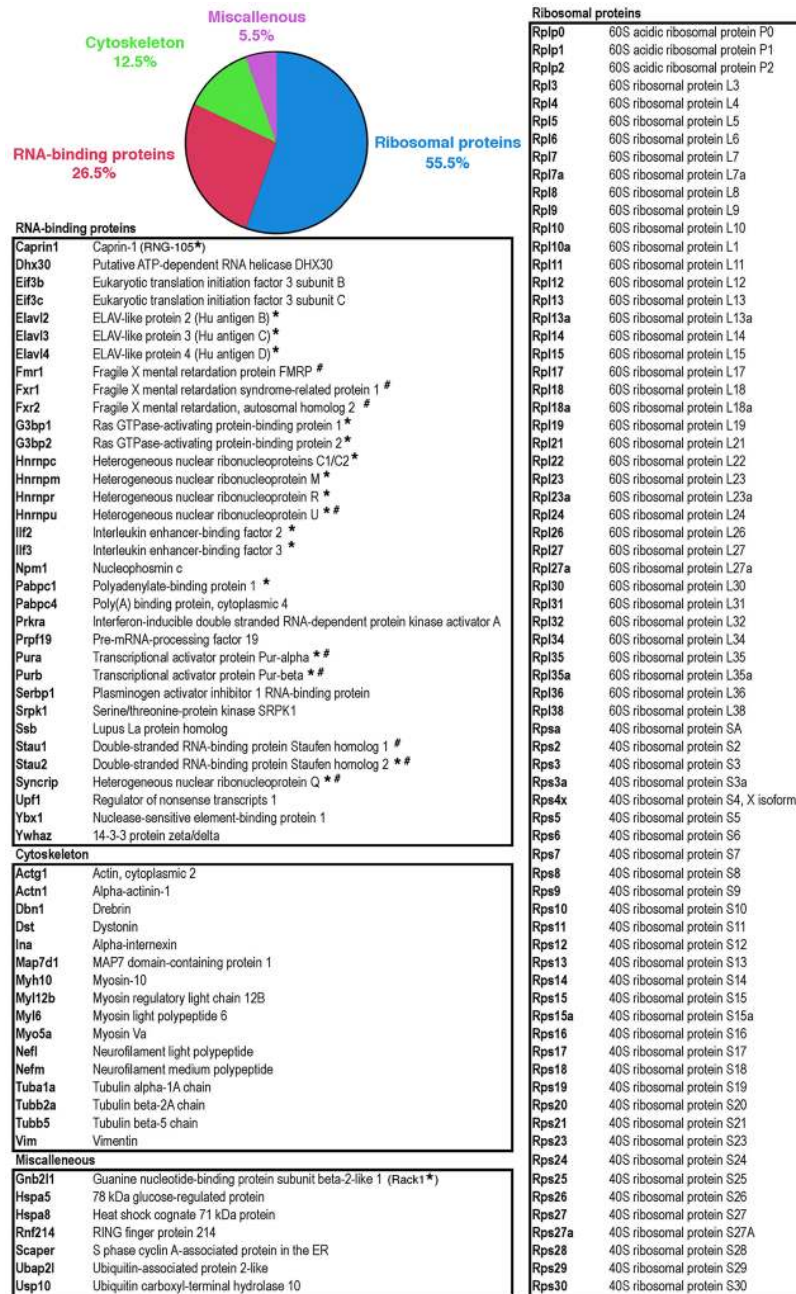
Pie chart categories:
- Miscellenous 5.5%
- Cytoskeleton 12.5%
- RNA-binding proteins 26.5%
- Ribosomal proteins 55.5%

RNA-binding proteins

Gene	Protein
Caprin1	Caprin-1 (RNG-105*)
Dhx30	Putative ATP-dependent RNA helicase DHX30
Eif3b	Eukaryotic translation initiation factor 3 subunit B
Eif3c	Eukaryotic translation initiation factor 3 subunit C
Elavl2	ELAV-like protein 2 (Hu antigen B) *
Elavl3	ELAV-like protein 3 (Hu antigen C) *
Elavl4	ELAV-like protein 4 (Hu antigen D) *
Fmr1	Fragile X mental retardation protein FMRP #
Fxr1	Fragile X mental retardation syndrome-related protein 1 #
Fxr2	Fragile X mental retardation, autosomal homolog 2 #
G3bp1	Ras GTPase-activating protein-binding protein 1 *
G3bp2	Ras GTPase-activating protein-binding protein 2 *
Hnrnpc	Heterogeneous nuclear ribonucleoproteins C1/C2 *
Hnrnpm	Heterogeneous nuclear ribonucleoprotein M *
Hnrnpr	Heterogeneous nuclear ribonucleoprotein R * #
Hnrnpu	Heterogeneous nuclear ribonucleoprotein U * #
Ilf2	Interleukin enhancer-binding factor 2 *
Ilf3	Interleukin enhancer-binding factor 3 *
Npm1	Nucleophosmin c
Pabpc1	Polyadenylate-binding protein 1 *
Pabpc4	Poly(A) binding protein, cytoplasmic 4
Prkra	Interferon-inducible double stranded RNA-dependent protein kinase activator A
Prpf19	Pre-mRNA-processing factor 19
Pura	Transcriptional activator protein Pur-alpha * #
Purb	Transcriptional activator protein Pur-beta * #
Serbp1	Plasminogen activator inhibitor 1 RNA-binding protein
Srpk1	Serine/threonine-protein kinase SRPK1
Ssb	Lupus La protein homolog
Stau1	Double-stranded RNA-binding protein Staufen homolog 1 #
Stau2	Double-stranded RNA-binding protein Staufen homolog 2 * #
Syncrip	Heterogeneous nuclear ribonucleoprotein Q * #
Upf1	Regulator of nonsense transcripts 1
Ybx1	Nuclease-sensitive element-binding protein 1
Ywhaz	14-3-3 protein zeta/delta

Cytoskeleton

Gene	Protein
Actg1	Actin, cytoplasmic 2
Actn1	Alpha-actinin-1
Dbn1	Drebrin
Dst	Dystonin
Ina	Alpha-internexin
Map7d1	MAP7 domain-containing protein 1
Myh10	Myosin-10
Myl12b	Myosin regulatory light chain 12B
Myl6	Myosin light polypeptide 6
Myo5a	Myosin Va
Nefl	Neurofilament light polypeptide
Nefm	Neurofilament medium polypeptide
Tuba1a	Tubulin alpha-1A chain
Tubb2a	Tubulin beta-2A chain
Tubb5	Tubulin beta-5 chain
Vim	Vimentin

Miscellaneous

Gene	Protein
Gnb2l1	Guanine nucleotide-binding protein subunit beta-2-like 1 (Rack1*)
Hspa5	78 kDa glucose-regulated protein
Hspa8	Heat shock cognate 71 kDa protein
Rnf214	RING finger protein 214
Scaper	S phase cyclin A-associated protein in the ER
Ubap2l	Ubiquitin-associated protein 2-like
Usp10	Ubiquitin carboxyl-terminal hydrolase 10

Ribosomal proteins

Gene	Protein
Rplp0	60S acidic ribosomal protein P0
Rplp1	60S acidic ribosomal protein P1
Rplp2	60S acidic ribosomal protein P2
Rpl3	60S ribosomal protein L3
Rpl4	60S ribosomal protein L4
Rpl5	60S ribosomal protein L5
Rpl6	60S ribosomal protein L6
Rpl7	60S ribosomal protein L7
Rpl7a	60S ribosomal protein L7a
Rpl8	60S ribosomal protein L8
Rpl9	60S ribosomal protein L9
Rpl10	60S ribosomal protein L10
Rpl10a	60S ribosomal protein L10a
Rpl11	60S ribosomal protein L11
Rpl12	60S ribosomal protein L12
Rpl13	60S ribosomal protein L13
Rpl13a	60S ribosomal protein L13a
Rpl14	60S ribosomal protein L14
Rpl15	60S ribosomal protein L15
Rpl17	60S ribosomal protein L17
Rpl18	60S ribosomal protein L18
Rpl18a	60S ribosomal protein L18a
Rpl19	60S ribosomal protein L19
Rpl21	60S ribosomal protein L21
Rpl22	60S ribosomal protein L22
Rpl23	60S ribosomal protein L23
Rpl23a	60S ribosomal protein L23a
Rpl24	60S ribosomal protein L24
Rpl26	60S ribosomal protein L26
Rpl27	60S ribosomal protein L27
Rpl27a	60S ribosomal protein L27a
Rpl30	60S ribosomal protein L30
Rpl31	60S ribosomal protein L31
Rpl32	60S ribosomal protein L32
Rpl34	60S ribosomal protein L34
Rpl35	60S ribosomal protein L35
Rpl35a	60S ribosomal protein L35a
Rpl36	60S ribosomal protein L36
Rpl38	60S ribosomal protein L38
Rpsa	40S ribosomal protein SA
Rps2	40S ribosomal protein S2
Rps3	40S ribosomal protein S3
Rps3a	40S ribosomal protein S3a
Rps4x	40S ribosomal protein S4, X isoform
Rps5	40S ribosomal protein S5
Rps6	40S ribosomal protein S6
Rps7	40S ribosomal protein S7
Rps8	40S ribosomal protein S8
Rps9	40S ribosomal protein S9
Rps10	40S ribosomal protein S10
Rps11	40S ribosomal protein S11
Rps12	40S ribosomal protein S12
Rps13	40S ribosomal protein S13
Rps14	40S ribosomal protein S14
Rps15	40S ribosomal protein S15
Rps15a	40S ribosomal protein S15a
Rps16	40S ribosomal protein S16
Rps17	40S ribosomal protein S17
Rps18	40S ribosomal protein S18
Rps19	40S ribosomal protein S19
Rps20	40S ribosomal protein S20
Rps21	40S ribosomal protein S21
Rps23	40S ribosomal protein S23
Rps24	40S ribosomal protein S24
Rps25	40S ribosomal protein S25
Rps26	40S ribosomal protein S26
Rps27	40S ribosomal protein S27
Rps27a	40S ribosomal protein S27A
Rps28	40S ribosomal protein S28
Rps29	40S ribosomal protein S29
Rps30	40S ribosomal protein S30

Fig 5. List of proteins detected in granules by mass-spectrometry. The pie chart reflects the main functional categories derived from the Gene Ontology analysis (S2 Table). Proteins labelled with * and # were previously identified in RNA granules [17,19 respectively].

doi:10.1371/journal.pgen.1006192.g005

Based on the results of the gene ontology analysis results, we sorted the proteins detected in granules according to the following functional classes: ribosomal proteins, RNA-binding proteins and cytoskeleton-linked proteins (Fig 5). Fifty five percent of the identified proteins were core ribosomal proteins (Fig 5). RNA-binding proteins constituted the second major class of proteins in granules (26.5%). Some of them were already described as part of RNA granules, such as polyA Binding Protein 1 and 4 (PABP1), members of the ELAV family (HuB, HuC),

Staufen1, Staufen2, Pur-α/β, series of heterogeneous ribonucleoproteins (hnRNPC1/C2; hnRNPR; hnRNPQ/SYNCRIP) and the Fragile X protein FMRP [16,17,19] (Fig 5). Also, several proteins known to interact directly with FMRP were detected, such as Caprin-1 [22] or the Fragile X-related proteins FXR1P and FXR2P [27]. Proteins, not previously described in RNA granules were also detected, such as the ATP-dependent helicase of the DEAD box family (DHX30) required for unwinding of mRNA during translation, and the translation initiation factors eIF3b and eIF3c. Other RNA-binding proteins were also present, for instance the splicing factors PRPF19, SRPK1 or UPF1. Finally, the presence of the axonal RNA-binding protein La suggested the presence of axonal granules in our preparations. Indeed, FMRP positive granules have been detected in axons [28,29]. Cytoskeleton-linked proteins represent 12.5% of the proteins identified in granules with a number of motor proteins (mostly myosins) and structural constituents of the cytoskeleton: actin, tubulin and neurofilaments (Fig 5).

The Fragile X Related proteins are enriched in granules

Using immunoblot analyses, we further tested the presence of a series of proteins detected in granules or polyribosomes namely: ribosomal proteins, translation factors and RNA-binding proteins. Equal amounts of proteins from granules or polyribosomes were analysed; we then compared the intensities of immunoblot signals. Levels of the core ribosomal proteins L7 and S6 in preparations of polyribosomes and of granules were similar. Reports of the presence of translation factors in granules are contradictory. Krichevsky and Kosik [16] observed that the granule fraction contained trace amounts of the initiation factors eIF4E and eIF4G1. On the other hand, Kanai et al. [19] detected eIF2A, eIF2B and eIF2G while Elvira et al. [17] reported the presence of eIF4A. In view of the absence of a consensus, we tested the presence of eIF4E, eIF4EBP1/e4BP1, eIF4G1 and eIF2A. All these factors were detected with equal signal intensities in both polyribosome and granule preparations (Fig 6A).

We further tested a series of RNA-binding proteins. We confirmed that PABP1 and Ago2 were equally represented in granules and polyribosomes (Fig 6A). In addition, we quantified signal intensities for the FXR proteins, FMRP, FXR1P and FXR2P. Contrary to the other RNA-binding proteins tested, FXR proteins signals were higher in granules when compared to polyribosomes (Fig 6B). Since quantification of chemiluminescent signals is not linear [30], we first determined the optimum conditions to ascertain the increased signals of FMRP in granules. We therefore checked, using a titration assay for FMRP, that our analyses were performed in the linear signal range (S4 Fig). In the case of FMRP, we quantified by densitometry analyses an increase of 1.83 fold in granules. These results are supported by our proteomics data, as the normalized spectral counts for the Fragile X Proteins appear higher in granules than polyribosomes (S1 Table). Finally, as controls, the post-synaptic protein PSD-95 and the mitochondria encoded cytochrome C oxidase MTCO1 were not detected in either of the preparations (Fig 6A) in agreement with the proteomic analyses.

Transcriptomic analyses of RNA granule preparations

Having studied the protein content of granules, we then wondered about their RNA content as compared to polyribosomes. To identify the RNA species present in granules, we compared RNA extracted from granules to polyribosomal RNA using whole transcriptome mouse microarrays. We focused on mRNA with signal intensities equal or higher than those from polyribosomes (Fold-of-Change (FC)>1, p-val<0.002). This corresponded to 1,806 annotated mRNAs (S4 Table) that can be assimilated to the mRNA species encountered in granules, corresponding to 7% of the total transcriptome. We performed gene ontology analysis to gain insights into the functional categories selectively over-represented in the granules (S5 Table). The biological
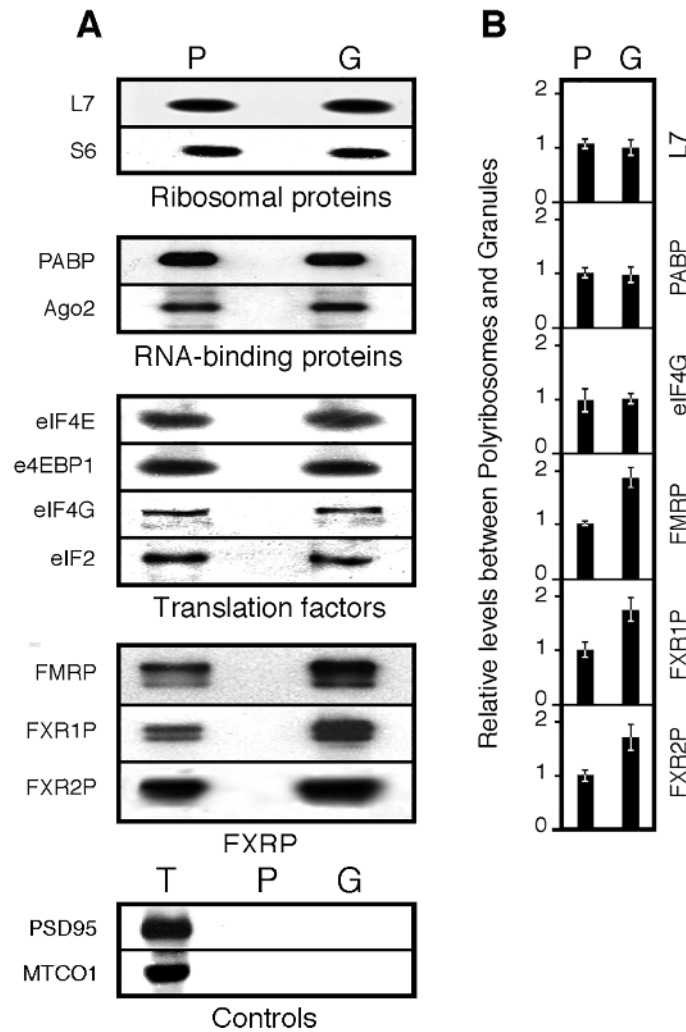
Fig 6. Comparative immunoblot analyses of selected proteins from polyribosomes and granules fractions. A) Immunoblot analyses of the steady state levels of selected proteins in polyribosomes (P) and in granules (G) and in total extract (T). **B)** Quantification of the signals. Mean values ± SEM of ratios calculated from 4 independent analyses.

doi:10.1371/journal.pgen.1006192.g006

processes enriched in granules mRNA were notably 'actin cytoskeleton organization' (adjusted pval = $6,16.10^{-8}$), 'cytoskeleton-dependent intracellular transport' (adjusted pval = $5,41.10^{-4}$), 'neuron projection development' (adjusted pval = $1,03.10^{-5}$), 'synapse organization' (adjusted pval = $7,54.10^{-4}$), 'axonogenesis' (adjusted pval = $5,5.10^{-4}$) or 'ubiquitin-dependent protein process' (adjusted pval = $2,16.10^{-3}$). In addition, the most enriched molecular functions concerned notably signal transduction pathways involving 'GTPase regulator activity' (adjusted pval = $7,47.10^{-8}$) or 'calcium ion binding' (adjusted pval = $8,62.10^{-8}$) or cytoskeleton-remodelling processes involving 'cytoskeletal protein binding' (adjusted pval = $1,81.10^{-15}$) or 'motor activity' (adjusted pval = $6,34.10^{-4}$). Finally, the most enriched cellular components included 'cytoskeleton' (adjusted pval = $7,21.10^{-19}$), 'axon' (adjusted pval = $1,87.10^{-12}$), 'growth cone' (adjusted pval = $3,48.10^{-6}$) 'synapse' (adjusted pval = $4,14.10^{-9}$) or 'dendrite' (adjusted pval = $7,26.10^{-9}$). All these processes are in line with the presumed functions of granules that are thought to transport mRNA dedicated to the regulation of synaptic development and

plasticity [31,32]. Considering the crucial role of FMRP in all these processes, we sought for overlap between the list of mRNA granules, and the previously published list of putative FMRP mRNA targets [33]. Interestingly, 15% of the mRNA listed in granules has been described as putative mRNA targets of FMRP (270 out of 1806, Fig 7A and S3 Table). Also, 32% of FMRP mRNA targets (270 out of 842, Fig 7A and S4 Table) are detected in RNA granules. These data support the important role played by FMRP in these structures.

To identify the specific subset of RNA preferentially transported in RNA granules, we focused on highly enriched mRNA (FC>4) as compared to polyribosomes. Interestingly, the mRNA *Map1b* encoding the microtubule-associated protein MAP1b, a transcript known to be targeted to the dendritic arborization [32] is enriched by a factor of 4 in granules (Fig 7B). The mRNA encoding αCaMKII, a known dendritic mRNA was not detected in our analyses since it is not yet expressed in brain of young mice [34]. A series of mRNA is enriched above 10 folds in granules in particular mRNAs encoding the cytoskeleton regulator Drebrin1, the myosin motor proteins Myo6 and Myh9, and a LIM-domain containing protein Limch1 (Fig 6 and S4 Table).

Granules and cargoes

While it has been reported that the granule size varies between 300 and 1000 nm [16], our electron microscopy results suggest that large granules might be composed of independent smaller granules of 100 to 300 nm in size (see Fig 3B to 3D). A plausible scenario would be that these independent granules fuse to form a "cargo of granules". In the case of FMRP, transfection studies of neurons in culture have shown the presence of GFP-tagged FMRP in travelling granules [35–38]. However, vectors used previously to express RNA-binding proteins in neuron primary cultures contain strong promoters, either from the cytomegalo-(CMV) or SV40-viruses, which result in high expression levels of the GFP-tagged RNA-binding proteins. Excess expression of RNA-binding proteins, in particular of FMRP, leads to the formation of cytoplasmic *foci* corresponding to stress granules (SG) [39]. We wish to point that, morphologically speaking, SG cannot *a priori* be discriminated from neuronal granules.

To ensure a neurospecific and more physiological expression of FMRP, we used the pShuttle-*GFP-FMR1* vector under the synapsin promoter. To investigate in living neurons the dynamics and kinetics of granules, we performed time-lapse video-microscopy experiments to follow the movements of GFP-FMRP in transfected cultured rat hippocampal neurons. We observed high levels of GFP-FMRP in the soma and proximal dendritic compartments, while smaller GFP-FMRP containing puncta were distributed throughout the distal dendritic arborisation (Fig 8A). In neurons grown for 7 days in culture, we noted a high proportion (42.8%, see below) of granules showing dynamic movements. The mean speed of these moving puncta was 0.123 ± 0.005 μm/s (calculated on n = 100 granules disseminated along 4 dendritic segments from 5 neurons). Interestingly, we regularly observed coalescing of GFP-FMRP puncta into larger ones, a phenomenon that has not been reported yet. Fig 8A and 8B (and S5 Fig) illustrate this phenomenon observed in two dendritic segments. In that neuron, we followed the fate of 70 GFP-FMRP puncta, 30 of which were moving distally from the soma, while the others had oscillatory movements. Among these moving puncta, 14 merged to form larger cargo-like structures. As shown in Fig 8A and 8B, four puncta fused to form a single larger one (an additional sequence of events is shown in S5 Fig). Distances travelled by each puncta along the X and Y axes are presented in Fig 8C. We quantified the moving speed of the individual puncta over a period of 20 min. In this example (detailed in Fig 8B to 8D), we observed 3 slow puncta (number 1,2 and 3) and a faster one. Of high interest, when the slow puncta merged, they kept a slow speed (puncta 2 and 3), while when the fast puncta fused with slow one, it appeared that
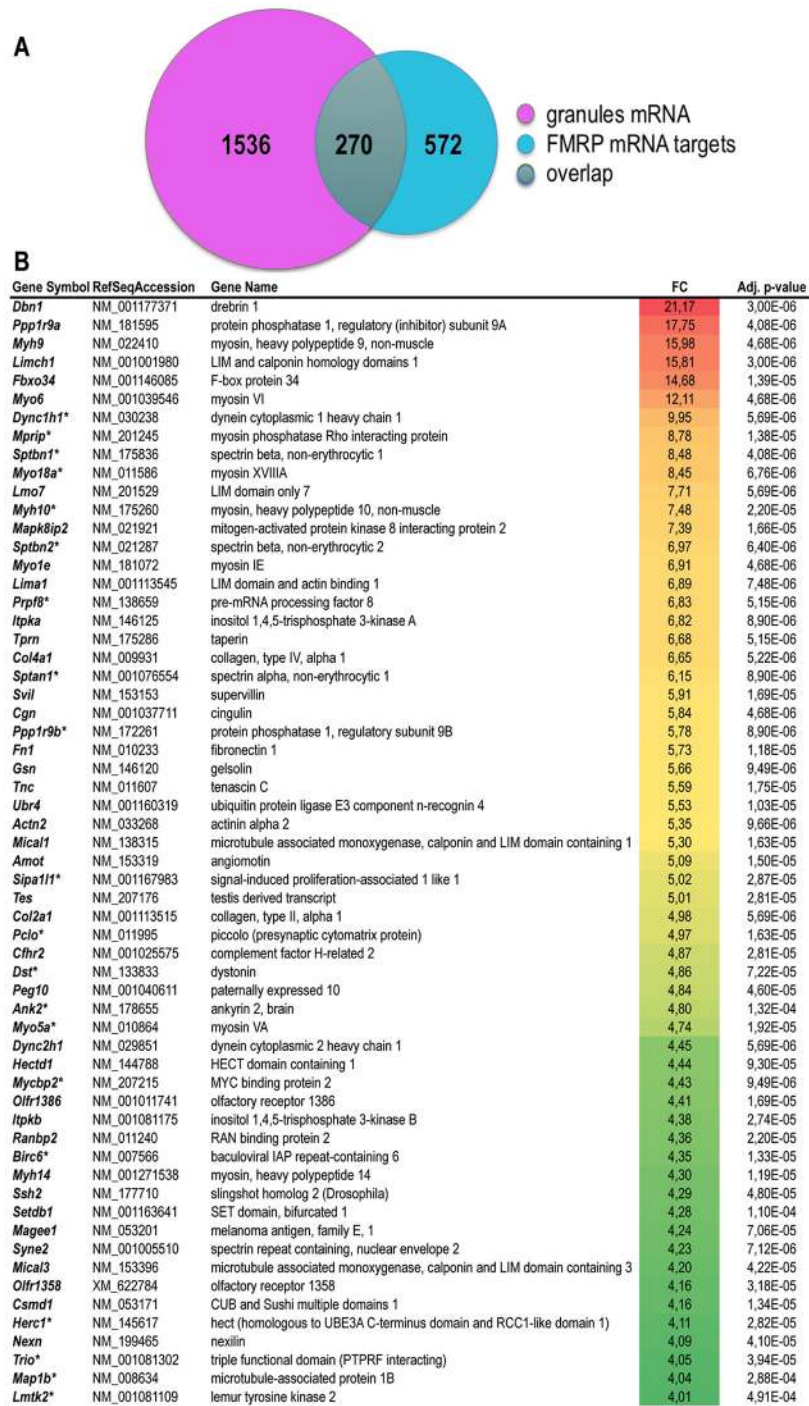
Gene Symbol	RefSeqAccession	Gene Name	FC	Adj. p-value
Dbn1	NM_001177371	drebrin 1	21,17	3,00E-06
Ppp1r9a	NM_181595	protein phosphatase 1, regulatory (inhibitor) subunit 9A	17,75	4,08E-06
Myh9	NM_022410	myosin, heavy polypeptide 9, non-muscle	15,98	4,68E-06
Limch1	NM_001001980	LIM and calponin homology domains 1	15,81	3,00E-06
Fbxo34	NM_001146085	F-box protein 34	14,68	1,39E-05
Myo6	NM_001039546	myosin VI	12,11	4,68E-06
Dync1h1*	NM_030238	dynein cytoplasmic 1 heavy chain 1	9,95	5,69E-06
Mprip*	NM_201245	myosin phosphatase Rho interacting protein	8,78	1,38E-05
Sptbn1*	NM_175836	spectrin beta, non-erythrocytic 1	8,48	4,08E-06
Myo18a*	NM_011586	myosin XVIIIA	8,45	6,76E-06
Lmo7	NM_201529	LIM domain only 7	7,71	5,69E-06
Myh10*	NM_175260	myosin, heavy polypeptide 10, non-muscle	7,48	2,20E-05
Mapk8ip2	NM_021921	mitogen-activated protein kinase 8 interacting protein 2	7,39	1,66E-05
Sptbn2*	NM_021287	spectrin beta, non-erythrocytic 2	6,97	6,40E-06
Myo1e	NM_181072	myosin IE	6,91	4,68E-06
Lima1	NM_001113545	LIM domain and actin binding 1	6,89	7,48E-06
Prpf8*	NM_138659	pre-mRNA processing factor 8	6,83	5,15E-06
Itpka	NM_146125	inositol 1,4,5-trisphosphate 3-kinase A	6,82	8,90E-06
Tprn	NM_175286	taperin	6,68	5,15E-06
Col4a1	NM_009931	collagen, type IV, alpha 1	6,65	5,22E-06
Sptan1*	NM_001076554	spectrin alpha, non-erythrocytic 1	6,15	8,90E-06
Svil	NM_153153	supervillin	5,91	1,69E-05
Cgn	NM_001037711	cingulin	5,84	4,68E-06
Ppp1r9b*	NM_172261	protein phosphatase 1, regulatory subunit 9B	5,78	8,90E-06
Fn1	NM_010233	fibronectin 1	5,73	1,18E-05
Gsn	NM_146120	gelsolin	5,66	9,49E-06
Tnc	NM_011607	tenascin C	5,59	1,75E-05
Ubr4	NM_001160319	ubiquitin protein ligase E3 component n-recognin 4	5,53	1,03E-05
Actn2	NM_033268	actinin alpha 2	5,35	9,66E-06
Mical1	NM_138315	microtubule associated monoxygenase, calponin and LIM domain containing 1	5,30	1,63E-05
Amot	NM_153319	angiomotin	5,09	1,50E-05
Sipa1l1*	NM_001167983	signal-induced proliferation-associated 1 like 1	5,02	2,87E-05
Tes	NM_207176	testis derived transcript	5,01	2,81E-05
Col2a1	NM_001113515	collagen, type II, alpha 1	4,98	5,69E-06
Pclo*	NM_011995	piccolo (presynaptic cytomatrix protein)	4,97	1,63E-05
Cfhr2	NM_001025575	complement factor H-related 2	4,87	2,81E-05
Dst*	NM_133833	dystonin	4,86	7,22E-06
Peg10	NM_001040611	paternally expressed 10	4,84	4,60E-05
Ank2*	NM_178655	ankyrin 2, brain	4,80	1,32E-04
Myo5a*	NM_010864	myosin VA	4,74	1,92E-05
Dync2h1	NM_029851	dynein cytoplasmic 2 heavy chain 1	4,45	5,69E-06
Hectd1	NM_144788	HECT domain containing 1	4,44	9,30E-05
Mycbp2*	NM_207215	MYC binding protein 2	4,43	9,49E-06
Olfr1386	NM_001011741	olfactory receptor 1386	4,41	1,69E-05
Itpkb	NM_001081175	inositol 1,4,5-trisphosphate 3-kinase B	4,38	2,74E-05
Ranbp2	NM_011240	RAN binding protein 2	4,36	2,20E-05
Birc6*	NM_007566	baculoviral IAP repeat-containing 6	4,35	1,33E-05
Myh14	NM_001271538	myosin, heavy polypeptide 14	4,30	1,19E-05
Ssh2	NM_177710	slingshot homolog 2 (Drosophila)	4,29	4,80E-05
Setdb1	NM_001163641	SET domain, bifurcated 1	4,28	1,10E-04
Magee1	NM_053201	melanoma antigen, family E, 1	4,24	7,06E-05
Syne2	NM_001005510	spectrin repeat containing, nuclear envelope 2	4,23	7,12E-06
Mical3	NM_153396	microtubule associated monoxygenase, calponin and LIM domain containing 3	4,20	4,22E-05
Olfr1358	XM_622784	olfactory receptor 1358	4,16	3,18E-05
Csmd1	NM_053171	CUB and Sushi multiple domains 1	4,16	1,34E-05
Herc1*	NM_145617	hect (homologous to UBE3A C-terminus domain and RCC1-like domain 1)	4,11	2,82E-05
Nexn	NM_199465	nexilin	4,09	4,10E-05
Trio*	NM_001081302	triple functional domain (PTPRF interacting)	4,05	3,94E-05
Map1b*	NM_008634	microtubule-associated protein 1B	4,04	2,88E-04
Lmtk2*	NM_001081109	lemur tyrosine kinase 2	4,01	4,91E-04

Fig 7. Overlap between mRNA present in granules and FMRP putative mRNA targets. A) Venn diagram presenting intersection between the list of mRNA present in granules listed in S4 Table (n = 1806) to the list of 842 putative FMRP mRNA targets identified by Darnell et al. [33]. **B)** List of mRNA selectively enriched in granules as compared to polyribosomes. Enrichment is calculated as the ratio in average probe intensity (fold-of-change, FC) in granules as compared to polyribosomes preparation. Only transcripts corresponding to probes displaying an enrichment above 4 (FC>2) with a significant adjusted pvalue (pval<0.002) are presented. In case of redundant probes targeting a single mRNA, data are provided for the probe providing the highest level of variation. The color code indicates the highest (red) to the lowest (green) folds of change detected. The asterisk (*) indicates putative FMRP mRNA targets identified by Darnell et al. [33].

doi:10.1371/journal.pgen.1006192.g007
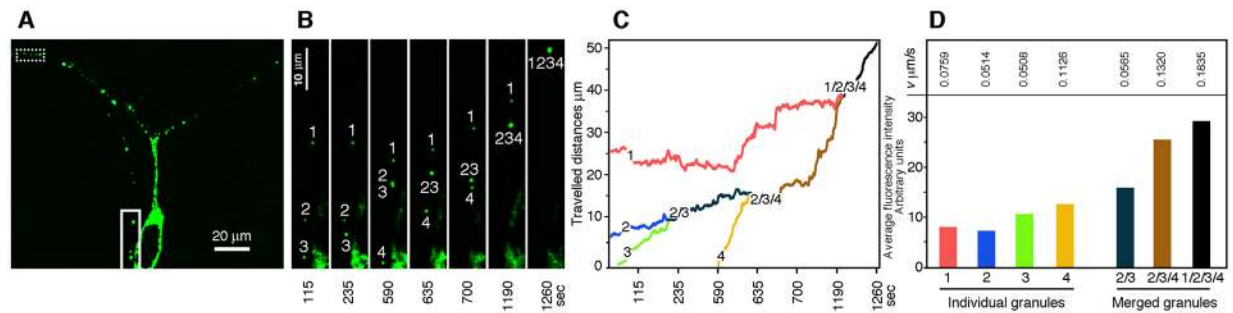
Fig 8. Traficking and merging of puncta into cargoes. A) GFP-FMRP is distributed in the somatodendritic compartment of a neuron in culture (DIV 7) transfected with the Syn-promoter driven GFP-FMRP expression vector. **B**) Insert at higher magnification, showing the movements of 4 independent puncta that finally merge into a large cargo. **C**) Trajectories and distance travelled by individual puncta across a 20 min period. **D**) Quantification of fluorescence intensity of each independent or merged puncta shown in **B**) and their respective speed.

the former imposed its faster momentum (Fig 8D). These observations were reproduced when following a set of 5 other puncta in a more distal area of the same neuron (see dashed box in Fig 8A and details in S5 Fig). Interestingly, the intensity of the fluorescent puncta increased as they merged, although not linearly, likely because of fluorescence quenching [40]. Altogether, these results are consistent with the existence of dynamic dendritic granules that can coalesce into cargoes as they move through the dendritic arborization.

How dendritic mRNAs are delivered to the synapse remains poorly understood. For instance, how could the narrow aperture of the spine neck, less than 200 nm in the case of hippocampal neurons [41,42], allows for the passage of the large granules described by Krichevsky and Kosik [16]. A plausible scenario would be that small granules are released from cargoes enabling their passage through the spine neck to reach the synaptic compartment. Interestingly, while tracking the movements of 221 puncta in different dendrites, we found 24 that moved out of the directional flow (see examples in Fig 9 arrow heads). We noticed small puncta budding from large fluorescent clusters, translocating through the neck into the spine head. Whether these structures corresponded to FMRP associated with the whole translation apparatus could not be determined and needs further analyses that are beyond the scope of the present study. However, since Antar et al. [36] have reported that only approximately 50% of FMRP colocalizes with ribosomal RNA and as we observed that not all granules contain FMRP (Fig 3G), we decided to determine to which extent FMRP colocalizes with the ribosomal marker L7 in dendrites. We performed immunofluorescence analyses on rat hippocampal neurons in primary cultures using IgY#C10 anti-FMRP and anti-L7 antibodies. Deconvolution and binary merging analyses of images using the MetaMorph Software enabled us to study L7 and FMRP colocalization in 4534 granules spread over 15 dendritic segments (Fig 10A). Several observations could be made from these colocalization studies. Firstly, the population of puncta positive for L7 is 2.5 fold larger than the FMRP one. Secondly, L7 and FMRP co-localize in 30% of the puncta. Thirdly, 60% of L7 positive granules were free of FMRP. Fourthly, FMRP positive puncta free of L7 represent 10% of the total puncta (Fig 10B). This last population that contains no ribosomes may serve as supply cargoes required to replenish and feed the translation machinery at the synapse, such as the translationally silent mRNPs containing CYFIP and FMRP [43].

Immunofluorescence studies have shown the huge heterogeneity of RNA-binding proteins contained in granules. Since we did not aim at establishing an exhaustive list of the many RNA-binding protein combinations present in the granules, we limited our studies to the FXR
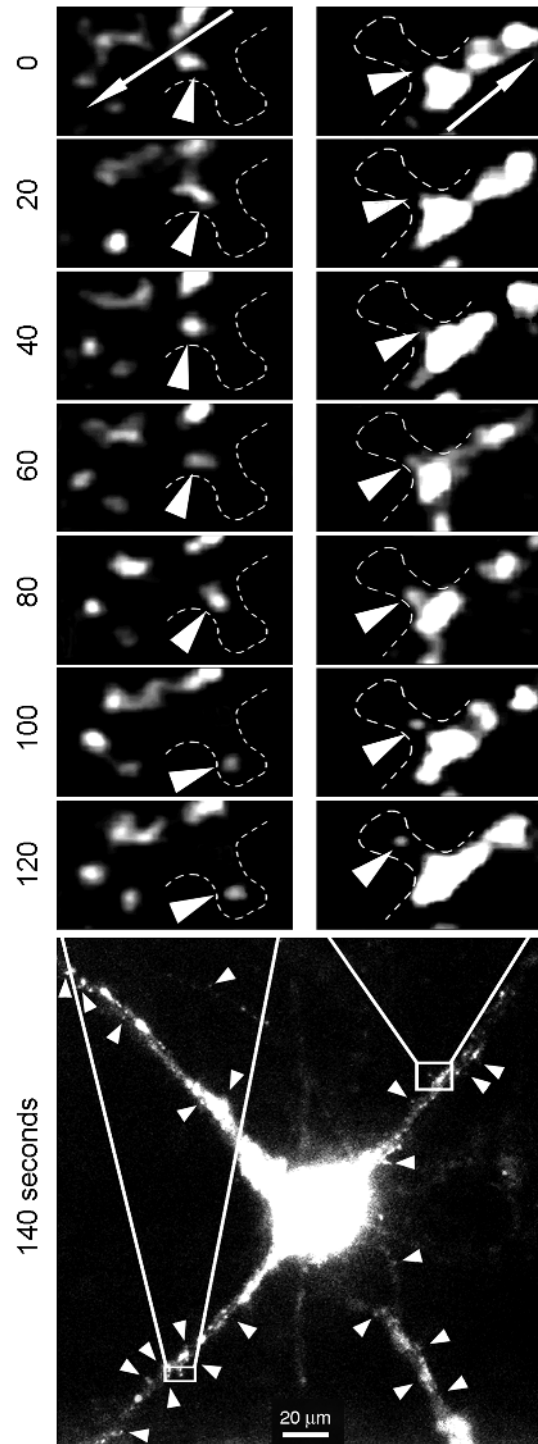
Fig 9. Translocation of small puncta into spines. Neurons (10–12 DIV) were transfected with the Syn-promoter driven GFP-FMRP expression vector. Time-lapse video microscopy showing small puncta emerging from large cargo-like structures and moving out of the dendrite main axis to reach the spine head. Arrows in the top insets indicate the anterograde flow movements. Arrow heads in the bottom image point to puncta emerging from the anterograde flow.
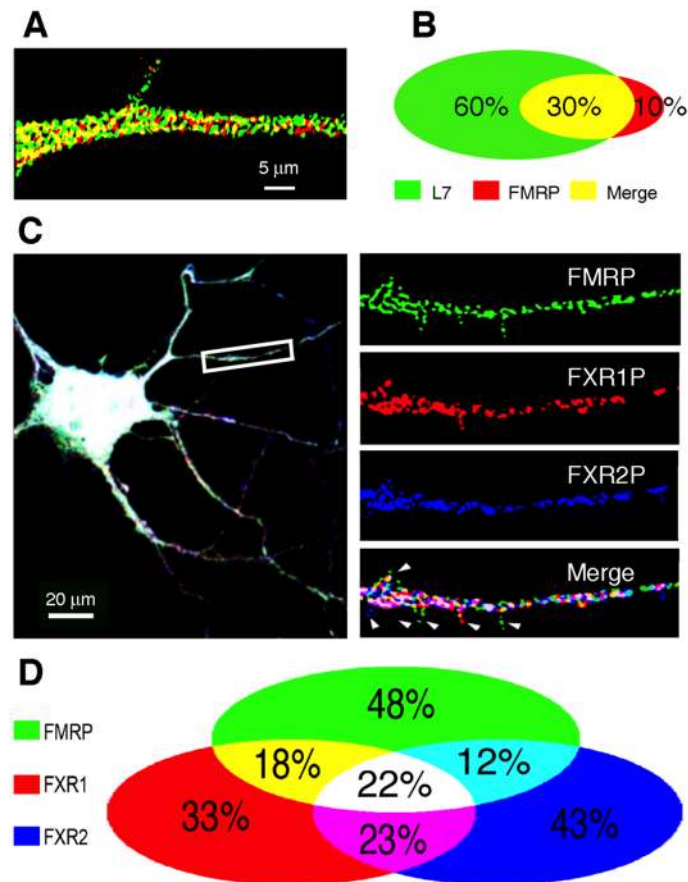
Fig 10. FMRP only partially co-localizes with the ribosomal protein L7 and members of the FXR family.
A) Double-immunofluorescence of FMRP (red) and L7 (green) showing that the majority of L7 does not co-localize with FMRP, while a minority of the latter **(B)** is free of L7. **C)** Co-localization of the three FXR protein members in dendritic granules of primary hippocampal neurons. Triple immunofluorescence of FMRP, FXR1P, and FXR2P, showing that all three members are present in dendritic granules, but do not always co-localize. Arrowheads point to granules containing a single FXR protein, presumably at the spines. **D)** Quantification and distribution of the three FXR protein members in dendritic granules shown in **(C)**.

doi:10.1371/journal.pgen.1006192.g010

family members. *In vitro*, all three members of this small family interact with each other to form homomers or heteromers [27] and have been detected in dendritic RNA granules after transfection of neurons with the respective expression vectors [44]. But so far, the coexistence of endogenous FMRP, FXR1P and FXR2P in the RNA granules has not been investigated. Therefore, we performed triple immunofluorescence labelling on hippocampal neurons in primary cultures (10 DIV) and studied the relative co-localization of the three endogenous FXR proteins (Fig 10C). We observed that 48% of FMRP-positive dendritic granules contain only FMRP, 43% of FXR2P-positive dendritic granules exhibit only FXR2P, while 33% of FXR1P-positive granules contain only FXR1P. Therefore, the FXR proteins are represented in various combinations, ranging from 12% to 23% of the granules that are double-labelled for two of the FXR proteins. Some granules exhibit only two members of the FXR family: 23% contain both FMRP and FXR2P or both FMRP and FXR1P and 12% show dual labelling for FXR1P and FXR2P. Interestingly, the three members of the family co-localize in only 22% of the granules (Fig 10D). These data are suggestive of the high level of diversity and heterogeneity in the composition of neuronal RNA granules.

Discussion

We report in the present study that we have isolated and characterized RNA granules from mouse brain in their second postnatal week of life. This developmental period correspond to active synaptogenesis while FMRP is abundantly expressed in the brain [45,46]. Despite the fact that the results reported here represent only a snapshot of the granule content at a specific time of neurodevelopment, they nevertheless contribute to shed light on several points and raise several conceptual issues.

Which proteins do make up granules?

Our high-resolution electron micrographs reveal an impressive and orderly morula-like architecture of granules resulting from densely packed polyribosomes. The proteomic analysis shows that 85.4% of the proteins identified in granules are also found in polyribosomes. While granules and polyribosomes share enriched pathways linked to 'translation', 'ribosome' and 'RNA-binding', cytoskeleton-linked terms appear only in RNA granule preparations. The latter data can be interpreted in two ways. On one hand, these proteins may represent trace contaminants from the cytoskeleton, which could remain in the fractions even after the Metrizamide purification step. On the other hand, they may be related to granule motility, as several myosin motors are represented. In particular, MyosinVa was previously described to transport major synaptic scaffolding proteins to dendritic spines [47].

Concerning the translation initiation and elongation factors in granules, our study documents the presence of eIF4E and eIF2a, in agreement with others [16,19]. We also report the identification a number of translation initiation factors IF3b, eIF3c, eIF4G as well as 4EBP1a and the RNA helicase DHX30. The presence in granules of the splicing regulators PRPF and SRPB1 seems a priory puzzling. However, the splicing factors and regulators, Nova-1 and Nova-2, are also present in the neuronal cytoplasm [48], where they control mRNA localization, stability and translation [49]. It is therefore plausible that PRPF and SRPB1 contribute to the localization and homeostasis of mature mRNA in neuronal cytoplasm and dendrites. Also intriguing is the presence of the argonaute family member Ago2, involved both in mRNA degradation and translation [50]. The diversity of the RNA-binding proteins identified in granules support the hypothesis that RNA granules might constitute a platform of local degradation or translation of mRNA transported at the synapse.

Using immunoblot analyses, we showed the presence of a series of proteins that were not detected by MS such as Ago2, eIF4E, e4EBP1, eIF4G, and eIF2A. The reason for this is not known. Interestingly, using MS, Elvira et al. [17] did not detect FMRP, or Pur α/β in granules while they were able to show the presence of these proteins by immunoblotting. It is possible that overrepresentation of ribosomal proteins may preclude adequate quantification or detection of other classes of proteins by MS. This might explain why some proteins are not detected. Alternatively, the relative abundances of some proteins may not be adequately reflected by normalized spectrum counts in proteomics versus immunoblotting analyses.

Proteomic analyses show that RNA granules contain both axonal and dendritic proteins. We believe that discrimination between dendritic and axonal granules is not possible when using total brain extract. The use of primary neurons grown in Campenot compartmentalized chambers [51] may allow such separation. It is not possible to conceive that all proteins described in the present study interact with each other in the same granule unit, neither it is envisioned that several mRNAs are targeted in the same granule. This is consistent with the fact that co-localization of different RNA-binding proteins in a single granule is not a general rule. Fig 10 shows that the FXRs only rarely colocalize *in vivo*, while the three members of the FXR family interact with each other *in vitro*. The same conclusions can be drawn for FMRP

and Caprin1 as they interact physically *in vitro*, while little co-localization is observed in dendritic granules [22]. Therefore we propose that each granule contains a single mRNA species with its dedicated RNA-binding protein(s) ensuring translation repression.

Which mRNAs are transported in granules?

Pathway enrichment analyses show that the transcripts present in granules are mainly associated with cytoskeleton-linked biological processes. In particular, the *Map1b* transcript, an identified FMRP target [33,52,53], is enriched at least 4-fold. Also, *Ppp1r9a* mRNA that codes the negative regulatory subunit of protein phosphatase-1 (PP1) is enriched over 16-fold in granules. The activation of PP1 is important for the induction of long-term depression (LTD), while its down regulation is required for the normal induction of long-term potentiation (LTP) of synaptic transmission [54]. Therefore, the fine-tuning of localized synthesis of PP1 regulatory subunit seems to modulate LTP and LTD locally at the synapse. LTP and LTD result from activity-dependent long-term adaptations of synaptic protein repertoire, in particular proteins involved in cytoskeleton remodelling. A strong enrichment (above 21-fold) of the F-actin and the microtubules modulator *Drebrin1* mRNAs suggests a crucial role for localized synthesis of the cognate protein. Indeed, Drebrin1 acts as a positive regulator of microtubule entry into spines [55], which plays a crucial role in synaptic function and plasticity. Also, mRNAs encoding LIM domain-containing proteins such as Limch1, Lmo7, Lima1, Mcal1 and Mcal3 are selectively enriched in granules preparations. LIM-domain containing proteins have been shown to play roles in cytoskeletal organisation, particularly at the synapse where their local synthesis would contribute to cytoskeleton remodelling, as described for LIM-domain containing kinase 1 [56].

What can we learn about FMRP's roles in granules?

In our granule preparations, we recovered approximately one third of the mRNA targets of FMRP described by Darnell et al. [33]. In addition, there is almost twice as much FMRP in granules than in polyribosomes. This speaks for a crucial role played by FMPR in these structures. Twenty putative mRNA targets of FMRP are enriched at least 4-fold in granules when compared to polyribosomes, indicating that these mRNAs are mainly targeted towards the dendritic compartment where they undergo localized synaptic translation regulated by FMRP, as is the case for *Map1b* [33,52,53]. The enrichment in granules of mRNA encoding motor proteins (*Dync1h1*, *Myo18a*, *Myh10*, *Myo5a*) described as targets of FMRP, raises the possibility that FMRP could address and modulate their local translation in dendrites and synapses, thereby controlling locally the movement of granules. In addition, the mRNA *Sptbn1*, *Sptbn2* and *Ank2*, the encoding members of the spectrin and ankyrin family that form a sub-membranous network involved in the regulation of synaptic stability and maintenance, are highly concentrated in granules and are putative mRNA targets of FMRP [33,57]. It is tempting to speculate that these mRNAs are addressed to the synapse and that dysregulation of their transport and local translation in the absence of FMRP contribute to the spine dysgenesis observed in Fragile X patients.

Where and how are granules formed?

We postulate that a class of granules emerge from stalled somatic polyribosomes [33,58] to form independent small RNA granules that are transported on microtubules, as is the case for granules carrying FMRP [36,59]. These small granules merge to form larger granules through a mechanism that has yet to be uncovered. Therefore, we propose the concept of RNA cargoes in which individual granules are recruited en route (Fig 11). Using time-lapse video microscopy,
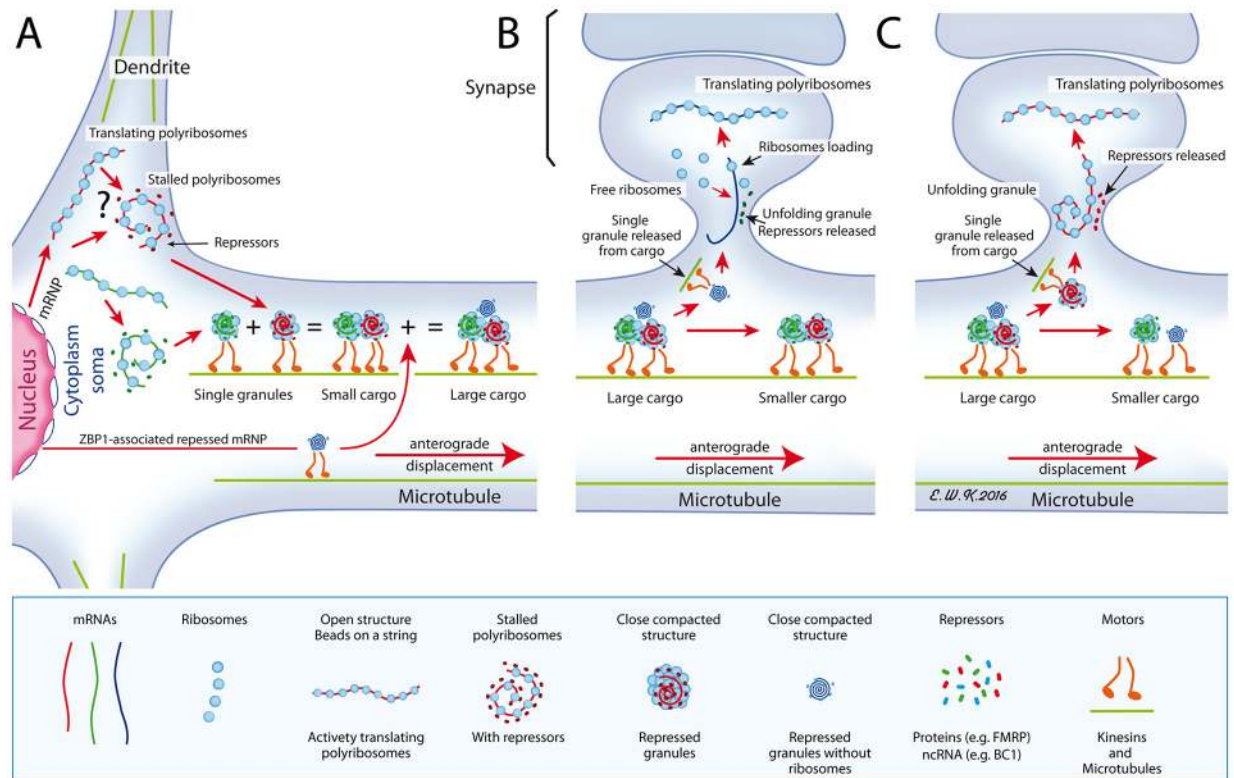
Fig 11. A proposed model for the formation of cargoes. A) Shown in the cytoplasm is the place of birth of granules that derive from stalled polyribosomes, in a close compacted structure. Alternatively (shown by an interrogation mark), polyribosomes might interact with yet unknown repressors (non coding RNA or proteins) to form granules that are transported to dendrites along microtubules, using motor proteins. Also, shown is a ZBP1-associated repressed RNP emerging from the nucleus. On their way, granules merge to form large cargoes. **B)** As large cargoes are too voluminous to cross the spine neck, individual small granules, in this instance the ZBP1-RNP devoid of ribosomes, emerge from cargoes and penetrate the narrow spine neck to join free ribosomes present in the post-synaptic area. **C)** A small granule containing the whole translation apparatus is translocated to the spine. In each instances, the close structure unfolds upon stimuli after releasing repressor molecules, either protein or RNA, to allow translation of its carried mRNA. Red lines with arrows indicate movements of the structures.

doi:10.1371/journal.pgen.1006192.g011

we observed small puncta coalescing into larger ones, suggesting that the so-called RNA granules can fuse into large cargoes of RNA granule entities. Forward movements display an average velocity of 0.123 ± 0.005 μm/sec, compatible with the reported speeds for granules labelled for GFP-Staufen (0.1 μm/sec [60]) and GFP-Pur-α (0.10–0.12 μm/sec [19]). Our tracking observation suggest that fast granules merging with slower granules, can impose their kinetics to the latter. This implies that each granule is under the control of a motor that determines its speed, and that once granules have merged, one specific motor determines the speed of the cargo. Importantly, FMRP interacts physically with members of the kinesin family [38,61] and immunoprecipitation studies have shown that it is present in complex brain structures containing the actin-based motor protein myosin Va and dynein [62] as well as KIF5A [19]. Furthermore, we detected in granules enriched mRNAs encoding motor proteins: myosins (*Myo1e*, *5a*, *6*, *18a and Myh9*, *10*, *14*) and dynein *Dync1h1*. Myo5a is required for the transport of FMRP mRNP [63] and associates with mRNP present in peripheral axons [64]. Myosin 10 is a motor involved in the formation of filopodia and development of dendritic spines and synapses in hippocampal neurons [65]. These data suggest that individual granules may be carried by different motors cooperating for their transport in the neuronal arborization [66,67]. It is also

possible that granules switch from microtubule to actin tracks to join other travelling granules, the nature of the motor of that switch being determined by the motor load [68].

How is the mRNA maintained as translationally silent in granules?

The resistance of granules to EDTA and RNase treatments strongly argues for a role of protein-protein interactions, rather than by protein-RNA links in maintaining the granule structure. This network of protein-protein interactions is dissociated by high-salt conditions, that remove certain RNA-binding proteins from brain polyribosomes [22]. Also, the association of these RNA-binding proteins with polyribosomes is sensitive to the anionic detergent deoxycholate that preserves only core polyribosomal proteins [20,21,23]. These observations support the hypothesis that dissociation of granules is conditioned by the removal of RNA-binding proteins, such as FMRP that is engaged into protein-protein interactions. This leads to the unfolding of the densely packed granule structure, which in turn can evolve towards the polyribosomes open structure (see below). Importantly, the close and compact structures described in the present study, have not been described in isolated polyribosomes that appear either as ring-shaped forms collapsed into double row structures or as linear polyribosomes densely packed into 3D helices [69,70]. Also, they have not been observed in organelles containing polyribosomes such as the Vault particles [71].

The present study provides converging evidence that mRNA present in granules is blocked once the translation initiation complex is formed. Firstly, the EM micrographs of granule preparations present striking similarities with those illustrating complexes of stalled polyribosomes [33]. Secondly, the compact-close structure of stalled polyribosomes is maintained even after EDTA or micrococal nuclease treatments [33], as is the case for the granules described in the present study. Thirdly, we confirmed by proteomic and immunoblotting analyses the presence in granules of several members of the translation initiation complex. These results are in line with a recent study performed in primary neuronal cultures revealing the presence of ribosome-bound nascent polypeptide chains budding from neuronal RNA granules, together with the RNA-binding proteins Staufen 2 and FMRP [58]. This suggests that neuronal mRNAs are transported in granules in the form of packed polyribosomes stalled after the first round of translation elongation.

A number of studies have shown that high levels of exogenous FMRP induce translation repression of reporter transcripts [39,72,73]. In addition, for the wide majority of well-characterized FMRP mRNA targets, the levels of the cognate protein are increased in the absence of FMRP. Finally, a landmark study from Darnell *et al.* [33] unveiled ribosomal stalling as an unexpected mode for translation repression by FMRP. We envision that FMRP functions as a translational repressor in RNA granules to prevent ectopic translation of its target mRNA during transport. Similarly, the orthologs FXR1P and FXR2P are enriched in granules in which they can be detected by immuno-electron microscopy. However their specific roles in translation regulation have been neglected so far.

How a large granule can cross the narrow neck of dendritic spines?

Because we showed that ribosomes are the basic unit of the granules, we postulate that the granule size is function of the number of ribosomes, presumably in relation itself to the length of the transported mRNA. Indeed, it has been hypothesized by Schuman et al. [74] that neuronal RNA granules exist as single entities and that each granule contains and transports a single mRNA. It results that, the longer the mRNA, the larger is the granule. The average size of a dendritic spine neck (200 nm [41,42]) represents a spatial constraint such that large RNA granules or cargoes cannot enter the synapse. In fact, as shown by our time-lapse video microscopy,

small granules might bud from large cargoes and pass through the neck into the spine. These observations lead us to speculate that once located in the spine, the translation apparatus is reactivated following adequate stimulations; in turn, the RNA-binding proteins or other repressors are released from the complex and are degraded. In the case of FMRP, it has been reported that mGluR activation leads to FMRP loss at the synapse [36] due to rapid degradation by the ubiquitin-proteasome pathway [75,76].

While our model predicts that a specific class of granules emerges from stalled polyribosomes, it does not rule out that other granular structures are formed in distinct cellular compartments. Indeed, the non-coding BC1 RNA, a translation repressor [13], is predominantly detected in dendritic granules and does not transit in polyribosomes [77]. Also, some granules might correspond to travelling repressed mRNPs, such as the ZBP1-associated mRNA complexes, that are formed in the nucleus [78,79].

Conclusions

The study of neuronal RNA granules have driven considerable attention since the discovery that the RNA-binding proteins FMRP, TDP-43, and SMN, respectively associated with Fragile X Syndrome [80], amyotrophic lateral sclerosis [81,82] and spinal muscular atrophy [83,84], are components of RNA granules. The primary morphological abnormality observed in the brain of Fragile X patients, is the presence of immature-looking dendritic spines [85] most likely resulting from alteration in the cytoskeleton architecture, as a consequence of defects in transport and translation of specific mRNA at the synapse. In the present study, we present evidence that travelling RNA granules are as heterogeneous as perhaps the whole extrasomatic transcriptome, and we hope that our approach will enable the in-depth study of dysregulations of RNA granules transport in neuropathologies. In the case of the Fragile X syndrome, we believe that the CLIP-RNAseq approach on granules preparations will enable to determine the precise nature of FMRP RNA targets addressed to the synapse, contributing to precisely reveal the defective mRNA involved in the syndrome.

Materials and Methods

Animals and neuronal primary cultures

C57BL/6J mice were bred in our animal facility and treated following the guidelines of the Canadian Council on Animal Care. The ethics committee of Université Laval has approved all procedures used in this study.

Hippocampal neuron cultures were prepared from neonatal rats as described [86]. Briefly, hippocampi were dissected out of postnatal day 1 rats. After dissociation, cells were washed, centrifuged and plated on poly-D-lysine-coated Aclar coverslips. Growth media consisted of Neurobasal supplemented with B27, penicillin/streptomycin (50 U/ml; 50 μg/ml), and 0.5 mM Glutamax (Thermo Fischer Scientific). Cytosine arabinofuranoside (Ara-C, 5 μM, Sigma) was added 2 days after plating to reduce the number of glial cells. After 4 days invitro, half of the growth medium was replaced with medium without Ara-C. Neurons were cultured between 7 and 13 DIV before use.

Preparation of brain polyribosomes and granules

Total brain cytoplasmic extracts were prepared from 10 days old C57BL/6J mice, using two different methods.

Extraction in buffer without detergent.   One brain (0.35 g) was homogenized in 3 ml of a buffer containing 20 mM Hepes (pH 7.4), 140 mM potassium acetate, 1 mM magnesium

acetate, and 1 mM EGTA, supplemented with protease and RNase inhibitors [18,19]. A third of the volume of the post-mitochondrial supernatant was analysed by sedimentation velocity in sucrose gradients.

Extraction in buffer with detergent. Three brains were homogenized in 9 ml of a buffer containing 20 mM Tris-HCl (pH 7.4), 150 mM NaCl, 2.5 mM MgCl$_2$, 1 mM DTT, 10 U/ml RNasine (Pharmacia), protease inhibitors (Mini Complete, Roche) and 50 μg/ml cycloheximide. A post-mitochondrial supernatant was obtained by centrifuging the homogenate at 9 000 g for 15 min. To concentrate polyribosomes, 1% Igepal CA-630 (Sigma Aldrich) was added to the post-mitochondrial supernatant and 8 ml of the solution were layered over a 2 ml pad made of 60% (w/v) sucrose in a 11 ml tube and centrifuged in a Beckman SW41 rotor at 34 000 rpm (avg 146 000g) for 2 hours at 4°C. The pellets were then resuspended in a 20 mM Tris-HCl pH 7.4, 150 mM NaCl, 2.5 mM MgCl$_2$ buffer for isokinetic analyses on sucrose gradients [20].

Isokinetic and isopycnic centrifugations

Sucrose density gradients. Linear sucrose density gradients were generated using the Gradient Mate (BioComp, Canada) according to the manufacturer's instructions. Unless specified in the results section, polyribosomes were analysed on 15–60% (w/v) isokinetic sucrose gradients made up in 20 mM Tris-HCl pH 7.4, 150 mM NaCl, 2.5 mM MgCl2. After centrifugation in a Beckman SW41 rotor for 2 hours at 34 000 rpm (avg 146 000g) and 4°C, gradients were fractionated by unloading from the top using the Auto Densi-Flow (Buchler) connected to an ISCO UA-5 flow-through spectrophotometer set at 254 nm. Each fraction was precipitated overnight at –20°C after addition of 2 volumes of ethanol. The precipitated material was collected by centrifugation in a microfuge at 12 000 rpm for 20 min and solubilized in SDS-sample buffer before immunoblot analyses [20].

Metrizamide gradients. Fractions containing polyribosomes and granules obtained after isokinetic centrifugation in sucrose gradients were diluted and/or resuspended in 20 mM Tris-HCl pH 7.4, 150 mM NaCl, 2.5 mM MgCl2 and centrifuged in a SW60 Ti rotor at 54 000 rpm (avg 300 000 g) at 4°C. Pellets were resuspended in 20 mM Tris-HCl pH 7.4, 150 mM NaCl, 2.5 mM MgCl2 and 0.8 ml samples layered over 3.8 ml preformed, linear 20–60% (w/v) Metrizamide, a non-ionic radiopaque contrast agent (Nyegaard, Oslo) gradients and centrifuged to equilibrium for 18 hrs at 43 000 rpm (avg 190 000 g) in a Beckman SW60.1 rotor. The bottom of each tube was punctured and 0.3 ml fractions were collected. Densities were determined from refractive index measurements [87,88] using an Erma Refractometer (Tokyo, Japan).

Protein analyses

Protein concentration was determined using the Bradford method after TCA precipitation of the extracted proteins and resolubilization in 0.2 N NaOH followed by neutralization with 0.2 N HCl. To adjust with accuracy the quantities of polyribosomal and granules protein loaded on SDS-PAGE, gels were stained with Coomassie Brilliant blue, scanned and total stained peaks integrated using the ImageJ program, and the loaded volumes consequently adjusted.

Protein were analysed by SDS-PAGE (10% acrylamide) and the resolved proteins stained with Coomassie brilliant blue. Resolved proteins were also transferred onto 0.45 μm nitrocellulose membranes (BioRad) and processed for immune-detection after blocking in 5% non-fat dry milk in PBS. The following primary antibodies were used: chicken anti-FMRP #C10 (dil 1:2000; [22]), mouse anti-FMRP mAb1C3 (1:2000; [89]), rabbit anti-FXR1P #ML13 (1:25000 [39]). Mouse anti-FXR2P mAb42 (1:2000), mouse anti-MTCO1 (1:2000, ab7291), rabbit anti-PSD95 (1:5000), mouse anti-α–Tubulin (1:5000, ab7291) were purchased from Abcam. Rabbit anti-L7 ribosomal protein (1:10000) was from Novus Biological; rabbit anti-S6 ribosomal

protein (1:2000), rabbit anti-PABP1 (1:1000), rabbit anti-eIF4G (1:1000), rabbit anti-eIF2A (1:1000) from Cell Signaling. Rabbit polyclonal anti-NeuroFilaments (1:1000, NF18934-1-AP) was from Proteintech. Mouse anti-Ago (1:500) from Upstate, rabbit anti-eIF4E (1:1000), and rabbit anti-e4EBP1 (1:1000) from Assay BioTech, and mouse anti-actin JLA-20 (1:1000) was obtained from Developmental Studies Hybridoma Bank (Iowa City, IA). Detection of bound antibodies was performed with HRP-coupled goat secondary antibodies to mouse or chicken or rabbit (Immunoresearch) followed by ECL reaction (Perkin Elmer) and exposure to Fuji X-ray films. Quantitation of signals was performed after scanning the films and analyses using the ImageJ software.

Immunofluorescence and live imaging

Hippocampal neurons grown on coverslips for 10-12DIV were processed for immunofluorescence. Rabbit anti-FXR1P #ML13, chicken anti-FMRP #C10, mouse anti-FXR2 and rabbit polyclonal anti-L7 primary antibodies were used at 10 times less than the dilutions used for immunoblot analyses (see above), followed by Alexa secondary antibodies (green, red, blue respectively). Samples were mounted in Prolong Gold medium (Invitrogen). Images were captured using a Zeiss LSM 510 confocal microscope and a 63x (1.4 NA) objective and analysed using the MetaMorph Software.

For time-lapse videomicroscopy experiments, hippocampal cultures were transfected using Lipofectamine as described [86] with the pShuttle/*GFP-FMR1* under the synapsin promotor, ensuring a neurospecific expression of FMRP. The vector was engineered by subcloning GFP-*FMR1* cDNA from pGFP-C2/FMRP construct [38] into the pShuttle (Stratagene) downstream of the synapsin promotor. Cells were imaged at 36°C–37°C in an open perfusion (0.2–0.5 ml/min) Qe-1 RC-41LP chamber (Warner Instruments) mounted onto a Zeiss Axiovert inverted microscope equipped with a 63x (1.4 NA) or 100x (1.3 NA) objectives. Images were captured with a cooled CCD camera (Cool Snap HQ, Roper Scientific) every 5 sec for 20 min. The intensities of fluorescence along the processes of each neuron were measured with a user-defined threshold with the MetaMorph software (Universal Imaging). The mean movements of granules were measured on a 20 minutes scale using the SpotTracker plugging of the ImageJ software (NIH, Bethesda).

Electron microscopy

Negative staining. Ten µl of polyribosome fraction were deposited on discharged, collodion-coated gold grids for 5 min. After washing the sample with ddH$_2$O, the grid was treated with 2% uranyl acetate for 2 seconds, the solution was removed, the grid washed with H$_2$0 and air-dried.

Immunogold labelling. The pelleted material obtained after isokinetic centrifugation was resuspended and concentrated by ultracentrifugation at 54 000 rpm (avg 300 000g) for 2 hours in 0.8 ml polyallomer tubes fitted in the Beckman SW60 Ti rotor using a Delrin adapter (Seton, CA). The obtained pellets were fixed *in situ* with 4% paraformaldehyde in PBS for 18 h at 4°C, dispersed in 3% low-gelling temperature agarose (37°C) in 0.1 M cacodylate buffer, pH 7.3. After cooling the solidified pellets were cut into blocks, dehydrated in a series of increasing ethanol concentrations, and then embedded in LR-White resin (London Resin Comp. UK). Ultrathin sections (70–90 nm) on formvar coated gold grids were preblocked in PBS-0.1% Tween 20 (PBST) containing 5% dry milk and reacted for 2 hours with rabbit anti-L7 and anti-S6 polyclonal antibodies, mouse mAb1C3 against FMRP, rabbit polyclonal ML13 against FXR1P, or mouse mAb42 against FXR2P. After washes with PBST, the grids were incubated with gold-labeled anti rabbit (15 nm) or mouse (5 nm) IgGs (BBI, Cedarlane, ON, Canada) in PBST-5%

dry milk for 1 hour at room temperature, washed with PBST, and postfixed with 1% glutaralde-hyde. Sections were stained with uranyl acetate and lead nitrate and examined in a JEOL 1200EX electron microscope at 80 kV.

Mass spectrometry and protein identification

Analyses were performed at the McGill University-Genome Québec Innovation Centre facility (Montréal, Canada). Fourty μg of proteins from granules or polyribosomes were run on an 11% acrylamide SDS-PAGE. Gels were stained with Coomassie blue and twenty gel slices per lane were excised. Proteins were digested *in situ* with trypsin, and the resulting tryptic peptides analysed by tandem mass spectrometry. All MS/MS spectra were analysed using Mascot [90] and X!Tandem [91]. Mascot was set up to search mouse proteome (Mus musculus released 2009/11/24) assuming non-specific digestion by trypsin. Mascot and X!Tandem were searched with a tolerance of 0.50 Da for both fragment and parent ion mass. Iodoacetamide derivatives of cysteine were specified in Mascot and X!Tandem as fixed modifications, while deamidation of asparagine and glutamine, methyl ester of aspartic acid and glutamic acid, methylation of cysteine and oxidation of methionine were specified in X! Tandem and Mascot as variable modifications. Scaffold software was used to validate MS/MS based peptide and protein identi-fications [92]. Peptide Prophet algorithm was used for peptide identification with a 95,0% con-fidence [93]. Protein identifications were accepted on the basis of at least 1 identified peptides. Protein probabilities were assigned by the Protein Prophet algorithm [94]. Proteins that con-tained similar peptides and could not be differentiated based on MS/MS analysis alone were grouped to satisfy the principles of parsimony. To provide a semi-quantitative appreciation of protein abundance, the dedicated function of Scaffold software was used to normalize individ-ual protein spectral counts data to the total spectral counts for each MS samples. The data pre-sented in S1 Table are scaled accordingly.

Microarray analyses

Total RNA from polyribosomes and granules from wild-type mice (n = 3 biological replicates) were extracted using Trizol LS (Invitrogen) according to the manufacturer's instructions. After DNase I digestion (Qiagen), RNA was further purified using RNeasy Mini kit (Qiagen). Quality and concentration of extracted RNA was measured using the 2100-Bioanalyzer (Agilent Tech-nologies, Palo Alto, CA, USA) with the RNA PicoLab Chip (Agilent Technologies). Only high-quality RNA (RIN over 8) was used for RNA amplification.

Thereafter, RNA was subjected to two rounds by T7 amplification using the RiboAmp HSPlus RNA Amplification Kit (Life Science, Foster City, CA, USA), purified and quantified using NanoDrop ND-1000 spectrophotometer (NanoDrop, Wilmington, DE, USA). Anti-sense-RNA (aRNA) samples were labelled with Cy3 or Cy5 using the Universal Linkage System (ULS) kit (Kreatech Diagnostic, Amsterdam, Netherlands) and 825 ng of labelled aRNA were hybridized on the SurePrint G3 Mouse GE 8x60K Microarray kit (Agilent) in a two-color dye-swap design in a hybridization oven for 17 h at 65°C. A simple direct comparison between treatments was done in full dye swap. Microarrays slides were then washed and scanned with the PowerScanner (Tecan, Männedorf, Switzerland) and analysed with the Array-Pro Analyzer software (MediaCybernetics, Bethesda, MD, USA).

Microarray data were pre-processed and analysed using the FlexArray 1.6.1 (http://genomequebec.mcgill.ca/FlexArray). Raw data correction consisted of a Lowess intra-array normalization and Quantile inter-array normalization. Statistically significant variations were detected using Limma (Bioconductor). Multiple hypotheses testing correction was done using the Benjamini-Hochberg procedure [95]. Differences in gene expression were evaluated by

calculating the fold of change (FC) of signal intensity in granules preparations versus polyribo-somal preparations. FC were considered significant when: i) net signal intensity is significantly over background in all arrays (technical and biological replicates); ii) the cut-off adjusted p-value <0.002 and iii) fold change reaches at least 1 (log2FC>0). Positive signal threshold was determined for each array from the average background value plus two standard deviations.

Gene ontology analyses

Gene ontology-based pathway analyses and downstream exploitation of protein and gene lists were performed using the freely available DAVID bioinformatics resources [96,97].

Supporting Information

S1 Fig. FXR1P and FXR2P are also present in granules as detected by immunogold label-ling (arrow heads for FXR1P; 15 nm and FXR2P; 5 nm) on LR-White resin embedded thin sections.
(TIF)

S2 Fig. Frequency distribution of gold-FMRP in 100 independent granules after immuno-gold-labelling on LR-White resin embedded sections.
(TIF)

S3 Fig. Isolation of polyribosome and RNA granule populations. A) Schematic diagram of the steps used for the purification of polyribosomes and granules. **B**) Isopycnic centrifugation on Metrizamide gradients reveals that granules and polyribosomes have identical density prop-erties.
(TIF)

S4 Fig. Titration assay to determine the steady state levels of FMRP in polyribosomes and granules. Ten and 20 μg of proteins from purified polyribosomes (P) and granules (G) were analysed in parallel by immunoblotting with IgY#C10, and the membrane exposed for different times to X ray films. Densitometric analyses enable to calculate that the ratio of 2 fold is observed with 10 μg loading and with a 20 sec exposure (underlined in the right panel). Quanti-tative analyses shown in Fig 6B in the main text, was performed under these conditions.
(TIF)

S5 Fig. Cargoes are formed by progressive coalescence of smaller puncta as observed by time-lapse video microscopy. A) Presented here is the second boxed area in Fig 8A in the main text (Top left) showing the movements of 5 independent granules. **B**) Individual trajecto-ries versus time of each of these granules.
(TIF)

S1 Table. Normalized spectrum counts for proteins identified by mass-spectrometry in granules and polyribosomes-enriched preparations. For each protein, individual spectrum counts normalized to the total spectrum counts are presented and ordered from the highest (red) to the lowest (green) values in granules preparations. A value of 0 indicates that the pro-tein was not detected. Official protein symbol and name, UniProt accession number and molecular weight (MW) are provided.
(PDF)

S2 Table. Gene Ontology analysis to reveal functional categories enriched in proteins iden-tified in granules (listed in Fig 5 and S1 Table). Analyses were performed using the DAVID bioinformatics resources with the granule list as input. GOTERM categories: biological

processes, cellular components and molecular functions with a significant Benjamini's adjusted pvalue (p<0.05) are presented.
(PDF)

S3 Table. Gene Ontology analysis to reveal functional categories enriched in proteins identified in polyribosomes (listed in S1 Table). Analysis was performed using the DAVID bioinformatics resources with the granule list as input. GOTERM categories: biological processes, cellular components and molecular functions with a significant Benjamini's adjusted pvalue (p<0.05) are presented.
(PDF)

S4 Table. List of mRNA detected in granules. For each transcript, probe and gene ID are provided. Enrichment is calculated as the logarithm (base 2) of the ratio in average probe intensity (log2FC) in granules as compared to polyribosomes preparation. Transcripts corresponding to probes displaying an enrichment equals or above 1 (FC>1; log2(FC)>0) with a significant adjusted pvalue (pval<0.002) are presented. In case of redundant probes targeting a single mRNA, data are provided for the probe providing the highest level of variation. The colour code indicates the highest (red) to the lowest (green) folds of change detected. Putative FMRP mRNA targets identified in Darnell et al. [33] are highlighted in green.
(PDF)

S5 Table. Gene Ontology analysis to reveal functional categories enriched in mRNA of the granules. Analysis was performed using DAVID bioinformatics resources with the list of transcripts with FC>1 and pval<0.002 (mRNA as abundant or more abundant in granules than polyribosomes, see S3 Table). GOTERM categories (biological processes, cellular components and molecular functions) with a significant Benjamini's adjusted pvalue (p<0.05) are presented.
(PDF)

Acknowledgments

Author Contributions

Conceived and designed the experiments: EWK PDK. Performed the experiments: LD REF ST XJ AD EWK. Analyzed the data: LD REF CR PDK EWK. Contributed reagents/materials/analysis tools: CR PDK. Wrote the paper: LD EWK. Corrected the paper: PDK.

References

1. Ramón y Cajal S. 1894. The Croonian lecture: la fine structure des centres nerveux. *Proceedings of the Royal Society of London* 55: 444–468.

2. Abbott LF, Nelson SB. 2000. Synaptic plasticity: taming the beast. *Nat Neurosci* 3: 1178–1183. PMID: 11127835

3. Sutton MA, Schuman EM. 2006. Dendritic protein synthesis, synaptic plasticity, and memory. *Cell* 127: 49–58. PMID: 17018276

4. Citri A, Malenka RC. 2008. Synaptic plasticity: multiple forms, functions, and mechanisms. *Neuropsychopharmacol* 33: 18–41.

5. Gerrow K, Triller A. 2010. Synaptic stability and plasticity in a floating world. *Curr Opin Neurobiol* 20: 631–639. doi: 10.1016/j.conb.2010.06.010 PMID: 20655734

6. Holt CE, Schuman EM. 2013. The central dogma decentralized: new perspectives on RNA function and local translation in neurons. *Neuron* 80: 648–657. doi: 10.1016/j.neuron.2013.10.036 PMID: 24183017

7. Koenig E. 1979. Ribosomal RNA in Mauthner axon: implications for a protein synthesizing machinery in the myelinated axon. *Brain Res* 174: 95–107. PMID: 487126

8. Steward O, Reeves TM. 1988. Protein-synthetic machinery beneath postsynaptic sites on CNS neurons: association between polyribosomes and other organelles at the synaptic site. *J Neurosci* 8: 176–184. PMID: 3339407

9. Martin R, Fritz W, Giuditta A. 1989.Visualization of polyribosomes in the postsynaptic area of the squid giant synapse by electron spectroscopic imaging. *J Neurocytol* 18: 11–18. PMID: 2709045

10. Job C, Eberwine J. 2001. Localization and translation of mRNA in dendrites and axons. *Nat Rev Neurosci* 2: 889–898. PMID: 11733796

11. Cajigas IJ, Tushev G, Will TJ, tom Dieck S, Fuerst N, Schuman EM. 2012. The local transcriptome in the synaptic neuropil revealed by deep sequencing and high-resolution imaging. *Neuron* 74: 453–466. doi: 10.1016/j.neuron.2012.02.036 PMID: 22578497

12. Kosik KS, Krichevsky AM. 2002. The message and the messenger: delivering RNA in neurons. *Sci STKE* 300: tr25.

13. Iacoangeli A. Tiedge H. 2013. Translational control at the synapse: role of RNA regulators. *Trends Biochem Sci* 38: 47–55. doi: 10.1016/j.tibs.2012.11.001 PMID: 23218750

14. Koenig E, Martin R. 1996. Cortical plaque-like structures identify ribosome-containing domains in the Mauthner cell axon. *J Neurosci* 16: 1400–1411. PMID: 8778291

15. Knowles RB, Sabry JH, Martone ME, Deerinck TJ, Ellisman MH, Bassell GJ, et al. 1996. Translocation of RNA granules in living neurons. *J Neurosci* 16: 7812–7820. PMID: 8987809

16. Krichevsky AM, Kosik KS. 2001. Neuronal RNA granules: a link between RNA localization and stimulation-dependent translation. *Neuron* 32: 683–696. PMID: 11719208

17. Elvira G, Wasiak S, Blandford V, Tong XK, Serrano A, Fan X, et al. 2006. Characterization of an RNA granule from developing brain. *Mol Cell Proteomics* 5: 635–651. PMID: 16352523

18. Aschrafi A, Cunningham BA, Edelman GM, Vanderklish PW. 2005. The fragile X mental retardation protein and group I metabotropic glutamate receptors regulate levels of mRNA granules in brain. *Proc Natl Acad Sci USA* 102: 2180–2185. PMID: 15684045

19. Kanai Y, Dohmae N, Hirokawa N. 2004. Kinesin transports RNA: isolation and characterization of an RNA-transporting granule. *Neuron* 43: 513–525. PMID: 15312650

20. Khandjian EW, Huot ME, Tremblay S, Davidovic L, Mazroui R, Bardoni B. 2004. Biochemical evidence for the association of fragile X mental retardation protein with brain polyribosomal ribonucleoparticles. *Proc Natl Acad Sci USA* 101: 13357–13362. PMID: 15329415

21. Stefani G, Fraser CE, Darnell JC, Darnell RB. 2004. Fragile X mental retardation protein is associated with translating polyribosomes in neuronal cells. *J Neurosci* 24: 7272–7276. PMID: 15317853

22. El Fatimy R, Tremblay S, Dury AY, Solomon S, De Koninck P, Schrader JW, et al. 2012. Fragile X mental retardation protein interacts with the RNA-binding protein Caprin1 in neuronal RiboNucleoProtein complexes. *PLoS ONE* 7: e39338. doi: 10.1371/journal.pone.0039338 PMID: 22737234

23. Khandjian EW, Corbin F, Woerly S, Rousseau F. 1996. The fragile X mental retardation protein is associated with ribosomes. *Nat Genet* 12: 91–93. PMID: 8528261

24. Ben-Shem A, Garreau de Loubresse N, Melnikov S, Jenner L, Yusupova G, Yusupov M. 2011. The structure of the eukaryotic ribosome at 3.0 A resolution. *Science* 334: 1524–1529. doi: 10.1126/science.1212642 PMID: 22096102

25. Hinton RH, Mullock BM, Gilhuus-Moe C-C. The use of Metrizamide for the fractionation of ribonucleoprotein particles. In: Methodological Developments in Biochemistry, volume 4, Subcellular Studies, pp 103–110 (edt Reid E.), Longman Group Limited, UK, 1973.

26. Dissous C, Lempereur C, Verwaerde C, Krembel J. 1976. The use of metrizamide as a density-gradient medium in studies of rat-liver polysomes. *Eur J Biochem*. 64: 361–367. PMID: 1278163

27. Zhang Y, O'Connor JP, Siomi MC, Srinivasan S, Dutra A, Nussbaum RL, et al. 1995. The Fragile X Mental Retardation Syndrome protein interacts with novel homologs FXR1 and FXR2. *EMBO J* 14: 5358–5366. PMID: 7489725

28. Price TJ, Flores CM, Cervero F, Hargreaves KM. 2006. The RNA binding and transport proteins staufen and fragile X mental retardation protein are expressed by rat primary afferent neurons and localize to peripheral and central axons. *Neuroscience* 141: 2107–2116. PMID: 16809002

29. Christie SB, Akins MR, Schwob JE, Fallon JR. 2009. The FXG: a presynaptic fragile X granule expressed in a subset of developing brain circuits. *J Neurosci* 29: 1514–1524. doi: 10.1523/JNEUROSCI.3937-08.2009 PMID: 19193898

30. Fournier C, Brons S, Taucher-Scholz G. 2003. Quantification of chemiluminescent signals using photon-sensitive films or a CCD camera. *Biotechniques* 35: 284–290. PMID: 12951769

31. Hirokawa N. 2006. mRNA transport in dendrites: RNA granules, motors, and tracks. *J Neurosci* 26: 7139–7142. PMID: 16822968

32. Dajas-Bailador F, Bonev B, Garcez P, Stanley P, Guillemot F, Papalopulu N. 2012. microRNA-9 regulates axon extension and branching by targeting Map1b in mouse cortical neurons. *Nat neurosci* 15: 697–699.

33. Darnell JC, Van Driesche SJ, Zhang C, Hung KY, Mele A, Fraser CE, et al. 2011. FMRP stalls ribosomal translocation on mRNAs linked to synaptic function and autism. *Cell* 146: 247–261. doi: 10.1016/j.cell.2011.06.013 PMID: 21784246

34. Burgin KE, Waxham MN, Rickling S, Westgate SA, Mobley WC, Kelly PT. 1990. In situ hybridization histochemistry of Ca^{2+}/Calmodulin-dependent protein kinase in developing rat brain. *J Neurosci* 10: 1788–1798 PMID: 2162385

35. Antar LN, Afroz R, Dictenberg JB, Carroll RC, Bassell GJ. 2004. Metabotropic glutamate receptor activation regulates fragile x mental retardation protein and FMR1 mRNA localization differentially in dendrites and at synapses. *J Neurosci* 24: 2648–2655. PMID: 15028757

36. Antar LN, Dictenberg JB, Plociniak M, Afroz R, Bassell GJ. 2005. Localization of FMRP-associated mRNA granules and requirement of microtubules for activity-dependent trafficking in hippocampal neurons. *Genes Brain Behav* 4: 350–359. PMID: 16098134

37. Antar LN, Li C, Zhang H, Carroll RC, Bassell GJ. 2006. Local functions for FMRP in axon growth cone motility and activity-dependent regulation of filopodia and spine synapses. *Mol Cell Neurosci* 32: 37–48. PMID: 16631377

38. Davidovic L, Jaglin XH, Lepagnol-Bestel AM, Tremblay S, Simonneau M, Bardoni B, et al. 2007. The fragile X mental retardation protein is a molecular adaptor between the neurospecific KIF3C kinesin and dendritic RNA granules. *Hum Mol Genet* 16: 3047–3058. PMID: 17881655

39. Mazroui R, Huot ME, Tremblay S, Filion C, Labelle Y, Khandjian EW. 2002. Trapping of messenger RNA by Fragile X Mental Retardation protein into cytoplasmic granules induces translation repression. *Hum Mol Genet* 11: 3007–3017. PMID: 12417522

40. Gautier I, Tramier M, Durieux C, Coppey J, Pansu RB, Nicolas JC, et al. 2001. Homo-FRET microscopy in living cells to measure monomer-dimer transition of GFP-tagged proteins. *Biophys J* 80: 3000–3008. PMID: 11371472

41. Sorra KE, Harris KM. 2000. Overview on the structure, composition, function, development, and plasticity of hippocampal dendritic spines. *Hippocampus* 10: 501–511. PMID: 11075821

42. Arellano JI, Benavides-Piccione R, Defelipe J, Yuste R. 2007. Ultrastructure of dendritic spines: correlation between synaptic and spine morphologies. *Front Neurosci* 1: 131–143. doi: 10.3389/neuro.01.1.1.010.2007 PMID: 18982124

43. Napoli I, Mercaldo V, Boyl PP, Eleuteri B, Zalfa F, De Rubeis S, et al. 2008. The fragile X syndrome protein represses activity-dependent translation through CYFIP1, a new 4E-BP. *Cell* 134: 1042–1054. doi: 10.1016/j.cell.2008.07.031 PMID: 18805096

44. Davidovic L, Tremblay S, Gravel M, De Koninck P, Khandjian EW. 2005. Fragile X Mental Retardation Protein: to be or not to be a translational repressor. In: *The Molecular Basis of Fragile X Syndrome*, Sung Y., and Denman R., eds. (Research Signpost), pp. 29–143.

45. Cook D, del Rayo Sanchez-Carbente M, Lachance C, Radzioch D, Tremblay S, et al. 2011. Fragile X Related Protein 1 clusters with ribosomes and messenger RNAs at a subset of dendritic spines in the mouse hippocampus. *PLoS ONE* 6(10): e26120. doi: 10.1371/journal.pone.0026120 PMID: 22022532

46. Davidovic L, Navratil V, Bonaccorso CM, Catania MV, Bardoni B, Dumas ME. 2001. A metabolomic and systems biology perspective on the brain of the fragile X syndrome mouse model. *Genome Res* 21: 2190–2202.

47. Yoshii A, Zhao JP, Pandian S, van Zundert B, Constantine-Paton M. 2013. A Myosin Va mutant mouse with disruptions in glutamate synaptic development and mature plasticity in visual cortex. *J Neurosc* 33: 8472–8482.

48. Racca C, Gardiol A, Eom T, Ule J, Triller A, Darnell RB. 2010. The Neuronal Splicing Factor Nova Co-Localizes with Target RNAs in the Dendrite. *Front Neural Circuits* 4: 5. doi: 10.3389/neuro.04.005.2010 PMID: 20407637

49. Störchel PH, Thümmler J, Siegel G, Aksoy-Aksel A, Zampa F, Sumer S, et al. 2015. A large-scale functional screen identifies Nova1 and Ncoa3 as regulators of neuronal miRNA function. *EMBO J* 34: 2237–2254. doi: 10.15252/embj.201490643 PMID: 26105073

50. Vasudevan S, Steitz JA. 2007. AU-rich-element-mediated upregulation of translation by FXR1 and Argonaute 2. *Cell* 128: 1105–1118. PMID: 17382880

51. Campenot RB, Lund K, Mok SA. 2009. Production of compartmented cultures of rat sympathetic neurons. *Nat Protoc* 4: 1869–1887. doi: 10.1038/nprot.2009.210 PMID: 20010935

52. Darnell JC, Jensen KB, Jin P, Brown V, Warren ST, et al. 2001. Fragile X mental retardation protein targets G quartet mRNAs important for neuronal function. *Cell* 107: 489–499. PMID: 11719189

53. Lu R, Wang H, Liang Z, Ku L, O'Donnell WT, Li W, et al. 2004. The fragile X protein controls microtubule-associated protein 1B translation and microtubule stability in brain neuron development. *Proc Natl Acad Sci USA* 101: 15201–15206. PMID: 15475576

54. Siddoway BA, Altimimi HF, Hou H, Petralia RS, Xu, Stellwagen D, et al. 2013. An essential role for inhibitor-2 regulation of protein phosphatase-1 in synaptic scaling. *J Neurosci* 33: 11206–11211. doi: 10.1523/JNEUROSCI.5241-12.2013 PMID: 23825423

55. Merriam EB, Millette M, Lumbard DC, Saengsawang W, Fothergill T, Hu X, et al. 2013. Synaptic regulation of microtubule dynamics in dendritic spines by calcium, F-actin, and drebrin. *J Neurosci* 33: 16471–16482. doi: 10.1523/JNEUROSCI.0661-13.2013 PMID: 24133252

56. Goellner B, Aberle H. 2012. The synaptic cytoskeleton in development and disease. *Dev Neurobiol* 72: 111–125. doi: 10.1002/dneu.20892 PMID: 21509946

57. Brown V, Jin P, Ceman S, Darnell JC, O'Donnell WT, et al. 2001. Microarray identification of FMRP-associated brain mRNAs and altered mRNA translational profiles in fragile X syndrome. *Cell* 107: 477–487. PMID: 11719188

58. Graber TE, Hebert-Seropian S, Khoutorsky A, David A, Yewdell JW, Lacaille JC, et al. 2013. Reactivation of stalled polyribosomes in synaptic plasticity. *Proc Natl Acad Sci USA* 110: 16205–16210. doi: 10.1073/pnas.1307747110 PMID: 24043809

59. Maghsoodi B, Poon MM, Nam CI, Aoto J, Ting P, Chen L. 2008. Retinoic acid regulates RARalpha-mediated control of translation in dendritic RNA granules during homeostatic synaptic plasticity. *Proc Natl Acad Sci USA* 105:16015–16020. doi: 10.1073/pnas.0804801105 PMID: 18840692

60. Kohrmann M, Luo M, Kaether C, DesGroseillers L, Dotti CG, Kiebler MA. 1999. Microtubule-dependent recruitment of Staufen-green fluorescent protein into large RNA-containing granules and subsequent dendritic transport in living hippocampal neurons. *Mol Biol Cell* 10: 2945–2953. PMID: 10473638

61. Dictenberg JB, Swanger SA, Antar LN, Singer RH, Bassell GJ. 2008. A direct role for FMRP in activity-dependent dendritic mRNA transport links filopodial-spine morphogenesis to fragile X syndrome. *Dev Cell* 14: 926–939. doi: 10.1016/j.devcel.2008.04.003 PMID: 18539120

62. Ohashi S, Koike K, Omori A, Ichinose S, Ohara S, Kobayashi S, et al. 2002. Identification of mRNA/protein (mRNP) complexes containing Puralpha, mStaufen, fragile X protein, and myosin Va and their association with rough endoplasmic reticulum equipped with a kinesin motor. *J Biol Chem* 277: 37804–37810. PMID: 12147688

63. Lindsay AJ, McCaffrey MW. 2014. Myosin Va is required for the transport of fragile X mental retardation protein (FMRP) granules. *Biol Cell* 106: 57–71. doi: 10.1111/boc.201200076 PMID: 24175909

64. Calliari A, Farias J, Puppo A, Canclini L, Mercer JA, Munroe D, et al. 2014. Myosin Va associates with mRNA in ribonucleoprotein particles present in myelinated peripheral axons and in the central nervous system. *Dev Neurobiol* 74: 382–396. doi: 10.1002/dneu.22155 PMID: 24272908

65. Lin WH, Hurley JT, Raines AN, Cheney RE, Webb DJ. 2013. Myosin X and its motorless isoform differentially modulate dendritic spine development by regulating trafficking and retention of vasodilator-stimulated phosphoprotein. *J Cell Sci* 126: 4756–4768. doi: 10.1242/jcs.132969 PMID: 23943878

66. Ali MY, Lu H, Bookwalter CS, Warshaw DM, Trybus KM. 2008. Myosin V and Kinesin act as tethers to enhance each others' processivity. *Proc Natl Acad Sci USA* 105: 4691–4696. doi: 10.1073/pnas.0711531105 PMID: 18347333

67. Gross SP, Vershinin M, Shubeita GT. 2007. Cargo transport: two motors are sometimes better than one. *Curr Biol* 17: R478–486. PMID: 17580082

68. Slepchenko BM, Semenova I, Zaliapin I, Rodionov V. 2007. Switching of membrane organelles between cytoskeletal transport systems is determined by regulation of the microtubule-based transport. *J Cell Biol* 179: 635–641. PMID: 17998399

69. Myasnikov AG, Afonina ZA, Ménétret JF, Shirokov VA, Spirin AS, Klaholz BP. 2014. The molecular structure of the left-handed supra-molecular helix of eukaryotic polyribosomes. *Nat Commun* 5: 5294. doi: 10.1038/ncomms6294 PMID: 25376914

70. Afonina ZA, Myasnikov AG, Shirokov VA, Klaholz BP, Spirin AS. 2015. Conformation transitions of eukaryotic polyribosomes during multi-round translation. *Nucleic Acids Res* 43: 618–628. doi: 10.1093/nar/gku1270 PMID: 25520190

71. Mrazek J, Toso D, Ryazantsev S, Zhang X, Zhou ZH, Fernandez BC, et al. 2014. Polyribosomes are molecular 3D nanoprinters that orchestrate the assembly of vault particles. *ACS Nano* 8: 11552–1159. doi: 10.1021/nn504778h PMID: 25354757

72. Laggerbauer B, Ostareck D, Keidel E-M, Ostareck-Lederer A, Fischer U. 2001. Evidence that fragile X mental retardation protein is a negative regulator of translation. *Hum Mol Genet* 10: 329–338. PMID: 11157796

73. Li Z, Zhang Y, Ku L, Wilkinson KD, Warren ST, Feng Y. 2001. The fragile X mental retardation protein inhibits translation via interacting with mRNA. *Nucleic Acids Res* 29: 2276–2283. PMID: 11376146

74. Schuman EM, Dynes JL, Steward O. 2006. Synaptic regulation of translation of dendritic mRNAs. *J Neurosci* 26: 7143–7146. PMID: 16822969

75. Hou L, Antion MD, Hu D, Spencer CM, Paylor R, Klann E. 2006. Dynamic translational and proteasomal regulation of fragile X mental retardation protein controls mGluR-dependent long-term depression. *Neuron* 51: 441–454. PMID: 16908410

76. Nalavadi VC, Muddashetty RS, Gross C, Bassell GJ. 2012. Dephosphorylation-induced ubiquitination and degradation of FMRP in dendrites: a role in immediate early mGluR-stimulated translation. *J Neurosci* 32: 2582–2587. doi: 10.1523/JNEUROSCI.5057-11.2012 PMID: 22357842

77. Brosius J, Tiedge H. 2001. Neuronal BC1 RNA: intracellular transport and activity-dependent modulation. *Results Probl Cell Differ* 34: 129–138. PMID: 11288672

78. Tiruchinapalli DM, Oleynikov Y, Kelic S, Shenoy SM, Hartley A, Stanton PK et al. 2003. Activity-dependent trafficking and dynamic localization of zipcode binding protein 1 and beta-actin mRNA in dendrites and spines of hippocampal neurons. *J Neurosci* 23: 3251–361. PMID: 12716932

79. Oleynikov Y, Singer RH. 2003. Real-time visualization of ZBP1 association with beta-actin mRNA during transcription and localization. *Curr Biol* 13: 199–207. PMID: 12573215

80. Kao DI, Aldridge GM, Weiler IJ, Greenough WT. 2010. Altered mRNA transport, docking, and protein translation in neurons lacking fragile X mental retardation protein. *Proc Natl Acad Sci USA* 107: 15601–15606. doi: 10.1073/pnas.1010564107 PMID: 20713728

81. Fallini C, Bassell GJ, Rossoll W. 2012. The ALS disease protein TDP-43 is actively transported in motor neuron axons and regulates axon outgrowth. *Hum Mol Genet* 21: 3703–3718. doi: 10.1093/hmg/dds205 PMID: 22641816

82. Alami NH, Smith RB, Carrasco MA, Williams LA, Winborn CS, et al. 2014. Axonal transport of TDP-43 mRNA granules in neurons is impaired by ALS-causing mutations. *Neuron* 81: 536–543. doi: 10.1016/j.neuron.2013.12.018 PMID: 24507191

83. Jablonka S, Bandilla M, Wiese S, Buhler D, Wirth B, Sendtner M, et al. 2001. Co-regulation of survival of motor neuron (SMN) protein and its interactor SIP1 during development and in spinal muscular atrophy. *Hum Mol Genet* 10: 497–505. PMID: 11181573

84. Zhang HL, Pan F, Hong D, Shenoy SM, Singer RH, Bassell GJ. 2003. Active transport of the survival motor neuron protein and the role of exon-7 in cytoplasmic localization. *J Neurosci* 23: 6627–6637. PMID: 12878704

85. Hinton VJ, Brown WT, Wisniewski K, Rudelli RD. 1991. Analysis of neocortex in three males with the fragile X syndrome. *Am J Med Genet* 41: 289–294. PMID: 1724112

86. Hudmon A, Lebel E, Roy H, Sik A, Schulman H, Waxham MN, et al. 2005. A mechanism for Ca^{2+}/calmodulin-dependent protein kinase II clustering at synaptic and nonsynaptic sites based on self-association. *J Neurosci* 25: 6971–6983. PMID: 16049173

87. Birnie GD, Rickwood D, Hell A. 1973. Buoyant densities and hydration of nucleic acids, proteins and nucleoprotein complexes in metrizamide. *Biochem Biophys Acta* 331: 283–294. PMID: 4590205

88. Rickwood D, Birnie GD. 1975. Metrizamide, a new density-gradient medium. *FEBS letters* 50: 102–110. PMID: 1112406

89. Devys D, Lutz Y, Rouyer N, Bellocq JP, Mandel JL. 1993. The FMR-1 protein is cytoplasmic, most abundant in neurons and appears normal in carriers of a fragile X premutation. *Nat Genet* 4: 335–340. PMID: 8401578

90. Koenig T, Menze BH, Kirchner M, Monigatti F, Parker KC, Patterson T, et al. 2008. Robust prediction of the MASCOT score for an improved quality assessment in mass spectrometric proteomics. *J Proteome Res* 7: 3708–3717. doi: 10.1021/pr700859x PMID: 18707158

91. Graig R, Beavis RC. 2004. TANDEM: matching proteins with tandem mass spectra. *Bioinformatics* 20: 1466–1467. PMID: 14976030

92. Searle BC. 2010. Scaffold: a bioinformatic tool for validating MS/MS-based proteomic studies. *Proteomics* 10: 1265–1269. doi: 10.1002/pmic.200900437 PMID: 20077414

93. Keller A, Nesvizhskii AI, Kolker E, Aebersold R. 2002. Empirical statistical model to estimate the accuracy of peptide identifications made by MS/MS and database search. *Anal Chem* 74: 5383–5392. PMID: 12403597

94. Nesvizhskii AI, Keller A, Kolker E, Aebersold R. 2003. A statistical model for identifying proteins by tandem mass spectrometry. *Anal Chem* 75: 4646–4658. PMID: 14632076

95. Hochberg Y, Benjamini Y. 1990. More powerful procedures for multiple significance testing. *Stat Med* 9: 811–818. PMID: 2218183

96. Huang da W, Sherman BT, Lempicki RA. 2009a. Bioinformatics enrichment tools: paths toward the comprehensive functional analysis of large gene lists. *Nucleic Acids Res* 37: 1–13.

97. Huang da W, Sherman BT, Lempicki RA. 2009b. Systematic and integrative analysis of large gene lists using DAVID bioinformatics resources. *Nat Protocols* 4: 44–57.